THE PENNSYLVANIA STATE UNIVERSITY
SCHREYER HONORS COLLEGE

DEPARTMENT OF BIOENGINEERING

CORRECTING THE STOKES-EINSTEIN-SUTHERLAND EQUATION

SAI KARTHIK SUNKARA
SPRING 2013

A thesis
submitted in partial fulfillment
of the requirements
for a baccalaureate degree
in Bioengineering
with honors in Bioengineering

Reviewed and approved* by the following:

Faculty Name: Erwin Vogler
Faculty Title: Professor
Thesis Supervisor

Faculty Name: Keefe Manning
Faculty Title: Associate Professor
Honors Adviser: Keefe Manning

* Signatures are on file in the Schreyer Honors College.

ABSTRACT

Implanting prosthetic devices or any device into the human body results in protein adsorption onto the surface of the material. This adsorption is one of the factors that determines whether or the body rejects the implanted device. Thus understanding protein adsorption kinetics is vital in the field of Biomaterials.

When a single protein solution comes into contact with a physical surface, an interphase layer is formed. The interphase layer expands due to the influx of protein molecules and then shrinks due to the efflux of water molecules. Eventually, the interphase comes to steady state with a finite volume. A similar set of events occur when a binary protein solution comes into contact with a surface but it is of interest to know which protein dominates the interaction. In Barnthip and Vogler's Biomaterials publication *Volumetric Interpretation of Protein Adsorption: Protein Adsorption Competition in a Binary Solution*, solution depletion and tensiometric experiments were conducted using various combinations of binary solutions. It was found that the selectivity follows a similar trend predicted by taking the diffusion coefficient ratio governed by the Stokes-Einstein-Sutherland (SES) equation.

When taking the diffusion coefficient ratio, it was assumed that the viscosity ratio is constant and can therefore be neglected in the SES equation. The resulting equation over predicted the selectivity for low molecular weight ratios and under predicted it for high molecular weight ratios. The goal of the project is to eliminate the discrepancy shown in the Barnthip publication by generating a modified form of the SES equation that is a good fit to the experimental data.

To generate an alternative form of the SES equation, an initial assumption was that the viscosity ratio is not constant due to the crowding effect near the interphase. This allows one to generate equations to model the viscosity ratio. Since the ratio is unknown, different models were considered.

To analyze the models, the curve fitting feature in SigmaPlot was utilized. Initially, an equation was generated and then coded into SigmaPlot. Then using the dynamic fit feature, the equation was fitted to the selectivity data. The obtained r-squared value and a qualitative inspection of the fit were used to determine the success of the model.

The viscosity ratio was modeled using the Einstein, Hatschek, and Cokelet viscosity models. But due to the poor correlation between the predicted selectivity values and the experimental data, these models were not further pursued. The ratio was then predicted using standard functions such as: y = a*x + b and y = a*exp(x), where y is the viscosity ratio and x is the molecular weight ratio. After the exponential form, y = a*x + b was substituted into the SES equation, the resulting equation was $\frac{C_j}{C_i} = ae^{-x}x^{-\frac{1}{3}} + b$. This equation yielded an r-squared value of 0.7376 and qualitatively followed the experimental data's trend. Thus it can be concluded that this equation modifies the SES equation to better fit the data. The new equation can be validated through the use of a cone and plate viscometer to measure the viscosity of the i^{th} and j^{th} protein at different concentrations in the future. Upon validation, the adsorption kinetics of a binary solution consisting of two dissimilar proteins can be predicted.

TABLE OF CONTENTS

LIST OF FIGURES

LIST OF TABLES

ACKNOWLEDGEMENTS

I would like to express my sincere gratitude to my research advisor, Dr. Erwin Vogler for his immense knowledge and patience to guide me through the initial phases of the thesis. Over the years that I spent working with Dr. Vogler, I gained more than just an appreciation to the field of Biomaterials and Surface Chemistry but also learned many lessons that are applicable in everyday life.

I would like to thank my committee: Dr. Peter Butler, Dr. William Hancock, and Dr. Keefe Manning. During Dr. Vogler's absence, I was very lost and did not make much progress on my thesis. I thank you for stepping in and providing me with both positive and negative feedback regarding the different drafts that I have sent you. Without your help, I would not have finished the thesis.

Chapter 1 : Introduction and Technical Background

The field of Biomaterials seeks to develop artificial materials used in medical devices that are intended to interact with biological systems. Some of the major problems in the field are the influence of surface chemistry on vicinal water, the relationship between the properties of vicinal water and protein activity on surfaces, and the relationship between protein activity and biological response to materials [1]. This project seeks to advance the understanding of protein activity on surfaces.

Medical devices such as implants, prosthetic devices, and surgical tools come into contact with the biological system. Typically, when a foreign material enters the human body, an immune response occurs and plasma proteins aggregate onto the surface of the material. Depending on the proteins that adsorb onto the surface, different types of cells attach to the proteins. Understanding protein adsorption may provide information regarding the rejection of implanted devices [2].

1-1: Adsorption

Absorption and adsorption are two fundamentally distinct concepts that can easily be confused. Absorption is a phenomenon that occurs when a fluid is dissolved in a solid or liquid [3], [4], [5], [6]. Adsorption, on the other hand, is the adherence of a substance to a physical surface. Also during absorption, the entire volume of the absorbed substance is involved, while a film is of the adsorbed substance is created on the surface during adsorption. Figure 1-1 is an illustration of absorption and adsorption.

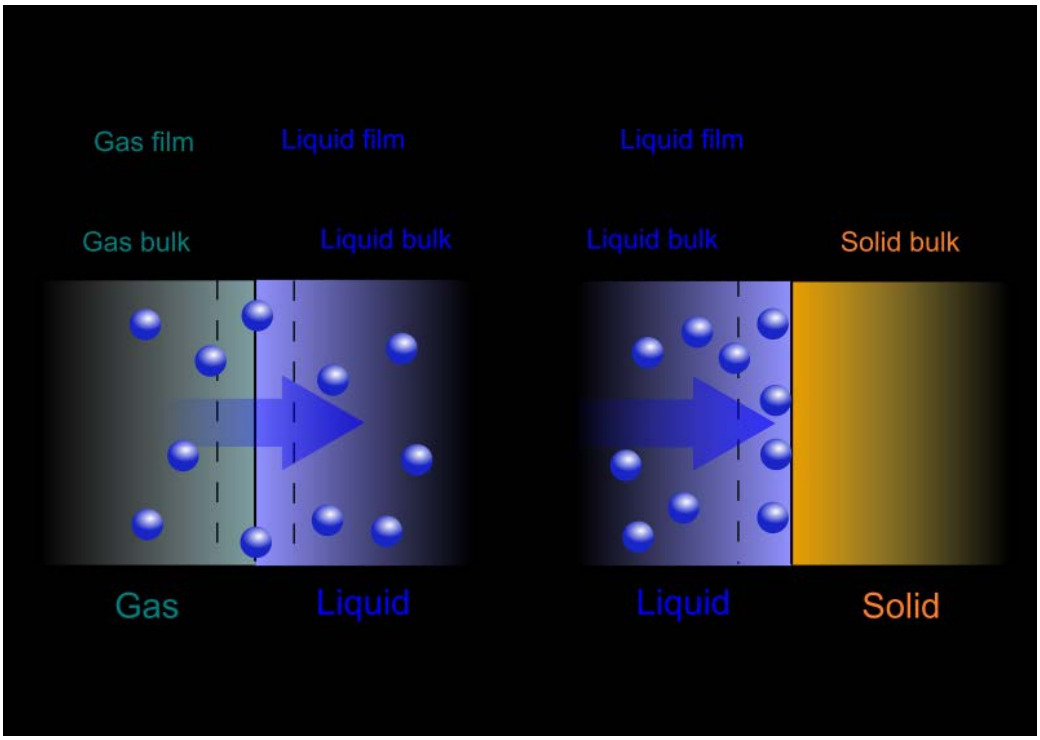

Figure 1-1: The fluid dissolves into the solid or liquid during absorption (left image), while in adsorption, a film of the adsorbate is deposited on the adsorbent (right image). Taken from [7].

1-2: Adsorption in the Interphase

Adsorption can be defined as the division of the bulk phase and an interphase – region between any two insoluble phases. When an adsorbate comes into contact with the adsorbent, an interphase region is formed. “Interphase” is used to highlight volumetric aspect that is involved with the boundary region. Therefore, it can be assumed that the interphase has a finite thickness [4].

There are two models of the interphase: Gibbs and Guggenheim [8], [9]. Gibbs’ model is more practical but not as intuitive as Guggenheim’s model. But both are useful models in surface science. The major difference between the two models is the way that the interphase is developed.

1-3: Guggenheim Phase Model

In real systems, there is a finite distance across an interface in which the properties gradually change from those of one adjacent bulk phase to those of the other [4]. Accordingly, one way of treating a surface is to consider it as a phase with a finite thickness and volume that is distinct from the adjacent bulk phases – see Figure 1-2 below.

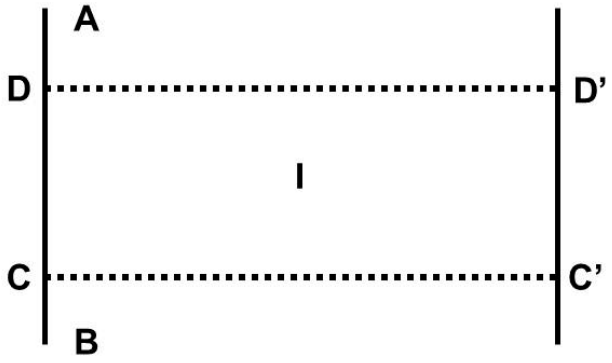

Figure 1-2: Guggenheim Phase Model shows that the interphase region labeled “I” contains both bulk solution A and B and has a finite thickness. Taken from [4].

The regions A and B are homogeneous bulk phases separated by the planar surface phase, I. Phases A and B are homogenous up to planes DD' and CC', respectively. The changes in properties from phase A to phase B take place in the region between CC' and DD', which has some arbitrary thickness [9].

1-4: The Gibbs Dividing Surface

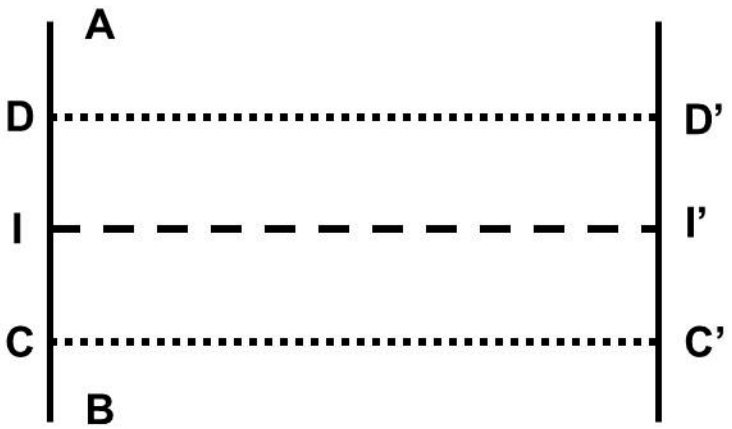

Figure 1-3: The Gibbs Dividing Surface model considers the presence of excess amount of fluid between planes DD' and CC'. The dividing surface II' was arbitrarily positioned. Taken from [4].

Gibbs considered the interface as a mathematical dividing plane. Phases A and B shown in Figure 1-3 are homogeneous up to planes DD' and CC', respectively. The dividing surface is designated as II'. Unlike Guggenheim's model, this region has no finite thickness or volume and is arbitrarily positioned between planes DD' and CC'. The amount of adsorption of component *i* is measured by its surface excess, defined as the amount of *i* in unit area of the region between AA; and BB' less the amount that there would be in the same region if A and B extended unchanged to II'. So the surface excess is the extra amount of a component in between DD' and CC' by virtue of the presence of the interface [8].

1-5: The Human Proteome

In the classic series entitled *The Plasma Proteins*, Putnam defined true plasma proteins as those that carry out their functions in the circulation. Proteins can be classified into different classes: Proteins Secreted by Solid Tissues and That Act in Plasma, Immunoglobulins, "Long Distance" Receptor Ligands, "Local" Receptor Ligands, Temporary Passengers, Tissue Leakage Products, Aberrant Secretions, and Foreign Proteins [5].

Hematological research, beginning with Franz Hofmeister's precipitation of bovine blood proteins with various salts, from the late 1800s to the early 1900s has led to the discovery of 30 different proteins in blood which are referred to as the "classical plasma proteins."[10] By 2000, about 490 proteins were identified using protein-separation methods, while more than 1000 blood proteins have been identified using combined chromatography and mass spectroscopy in the last decade [11].

The 5 most abundant proteins excluding hemoglobin are: Albumin, Total IgG, Fibrinogen, Transferrin, and IgA. The abundance of proteins in plasma varies significantly. Albumin is very abundant with a normal concentration range of 35-50 mg/mL, while interleukin with a normal concentration range of 0-5 pg/mL is not very abundant. These two proteins differ in plasma abundance by a factor of 10^{10} and can both be measured in a laboratory shows the progress of current immunoassay technology [11]. Figure 1-4 shows the normal concentration ranges of the proteins – the concentration decreases as the plot moves from the classical plasma proteins to the interleukins.

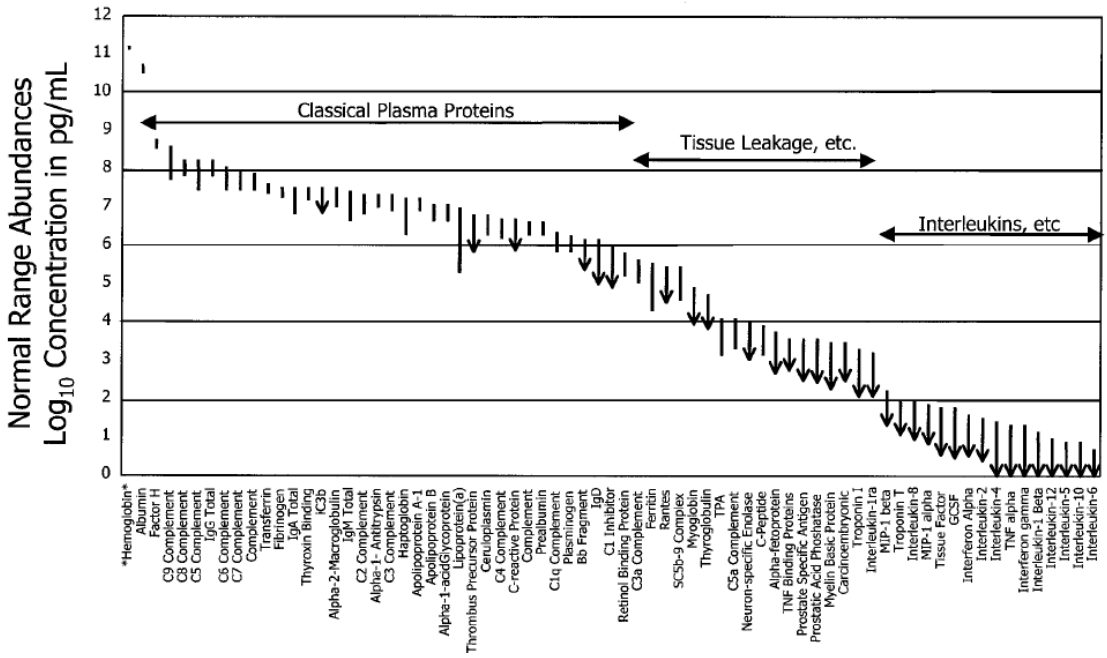

Figure 1-4: The abundance of the proteins has been grouped into three categories: Classical Plasma Proteins, Tissue Leakage, and Interleukins Taken from [11].

1-6: Proteins are Spheres in Solution

Proteins can be approximated to be treated as spheroids when the partial specific volume, v°, is in the range of 0.70 and 0.75 cm^3g^{-1}. A polypeptide chain has a spherical radius, r_v, between 1 and 7 nm to result in the globular shape. The spherical radius of a protein can be found using the relationship: $r_v = 6.72 \times 10^{-8} MW^{1/3}$. Using the spherical radius, it can be said that the protein volume is proportional to the molecular weight. It can be shown that v° = 0.77 cm^3/g (refer to Appendix A), which is just outside of the experimental range would correspond to a perfectly spherical protein [12-16].

Proteins are polyelectrolytes with an excluded volume surrounding the protein that forms an osmolaric barrier to the overlapping of hydration shells. In Figure 1-5, the excluded radius (not shown) is approximated 1/3 larger than the spherical radius. The net radius of a protein sphere R = 1.3 r_v [17].

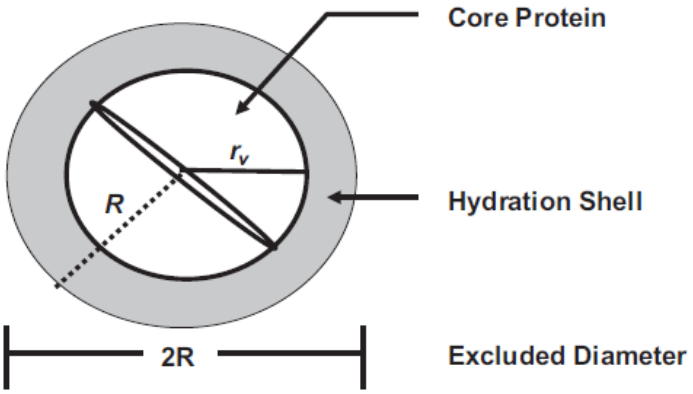

Figure 1-5: A protein can be treated as a hydration sphere when its specific volume is between 0.70 and 0.75 cm^3g^{-1} Taken from [17].

1-7: Role of Water in Protein Adsorption

When water comes into direct contact with an adsorbent surface, it is physicochemically bound to the surface. A network is formed by the hydrogen bonding of local water molecules to the neighboring water molecules. Vicinal water molecules that are bound to the adsorbent surface are also bound to adjacent water molecules. This implies that water in the interphase region is bound to the adsorbent surface – the adsorbent surface energy determines the extent to which the water molecules are bound to the surface. [17] – [20]

It is important to think about the energetics involved with displacing a finite volume of water because when a protein that is adsorbing onto a surface displaces water, there will be energetic consequences. The volume of displaced water is dependent upon:

1) Protein size as described
2) The number of protein layers that are occupied in the adsorbed state, which is dependent solution concentration and the molecular weight of the protein
3) The manner in which the protein molecules are organized in the adsorbed layers.

As a result, water is a driving force in protein adsorption [17].

1-8: Gedanken Model

The five most abundant blood proteins excluding hemoglobin are: serum albumin (HSA, 66.3 kDa, ~45, mg/mL), total various forms of immunoglobulin G (IgG, 160 kDa, ~10 mg/mL), fibrinogen (Fib, 341 kDa, ~3 mg/mL), transferrin (Tr, 77 kDa, ~ 3 mg/mL), and total immunoglobulin A (IgA, 160 kDa, ~ 1 mg/mL). A hypothetical cube can be constructed while visualizing these abundant proteins in plasma. In Figure 1-6, a 50 x 50 x 50 nm cube with the relative sizes of the abundant proteins is shown. It can be determined from an inspection of the figure that the concentration of larger (higher molecular weight) proteins is less than that of smaller (lower molecular weight) proteins. Adsorption is dominated by HSA strictly based on the concentrations described above and Figure 1-6 [17].

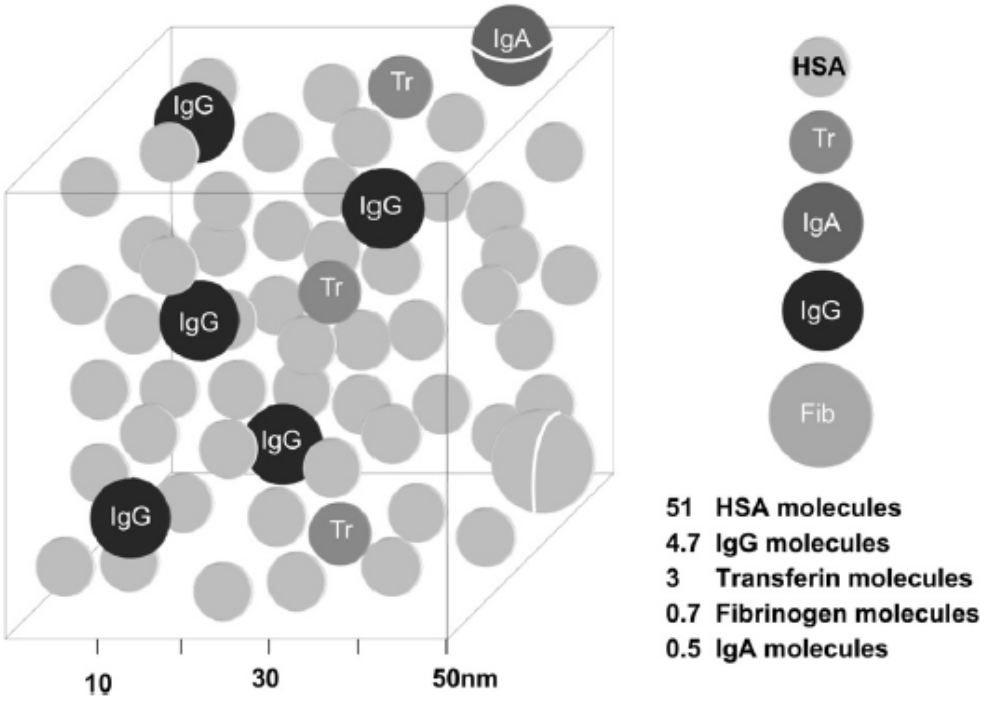

Figure 1-6: The Gedanken Model shows that there is an increase in the number of protein molecules with decreasing protein size. Taken from [17].

1-9: Introduction to the kinetics of protein adsorption

The kinetics of protein adsorption are of importance in the field of biomaterials the rate of protein adsorption is a factor in the selective adsorption that is seen in a binary solution or a multi-component solution. It is commonly thought that the Vroman Effect, which states that low molecular weight proteins arrive at the interphase first and then are displaced by higher molecular weight proteins, explains the selectivity [18]. But the validity is of this theory is questionable.

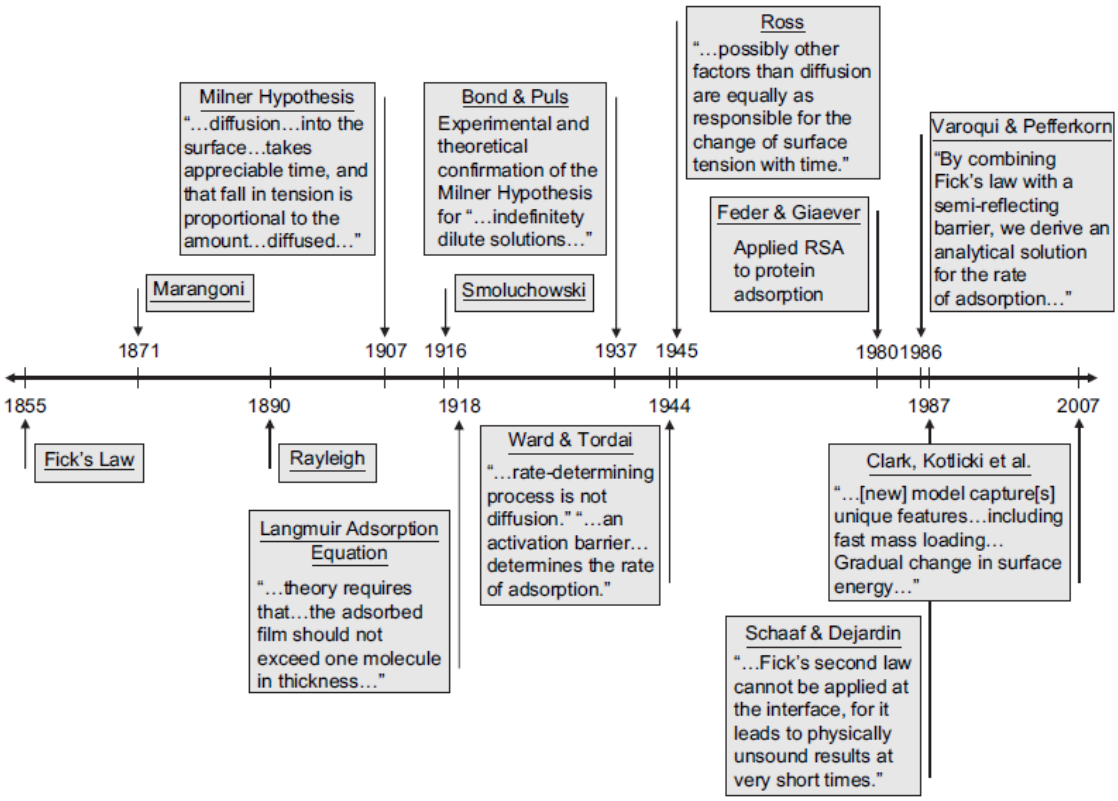

Figure 1-7: The study of adsorption kinetics has been of interest for several decades. A timeline of selected history of research is shown. Taken from [21].

As depicted by Figure 1-7, adsorption kinetics has been studied actively for many decades. An early conclusion that was drawn was that diffusion and mass transfer are not the only factors that control the adsorption rates. This was rationalized by Fick's law, which states that protein adsorption should come to equilibrium in milliseconds [19]. So the rate of appearance of a surfactant on a surface is too slow to be controlled by diffusion.

As a result of the discrepancy between measured rates and diffusion theory, physical chemists proposed that surfactant molecules must overcome an energy barrier to become adsorbed and that the height of this energy barrier controlled adsorption rates. Figure 1-8 shows a physical description of this imaginary energy barrier, which is also

referred to as the reflecting plane because it can repel surfactant molecules arriving from bulk solution. It is known that not every encounter with the surface leads corresponds to adsorption, which is accounted for by the energy barrier concept [20].

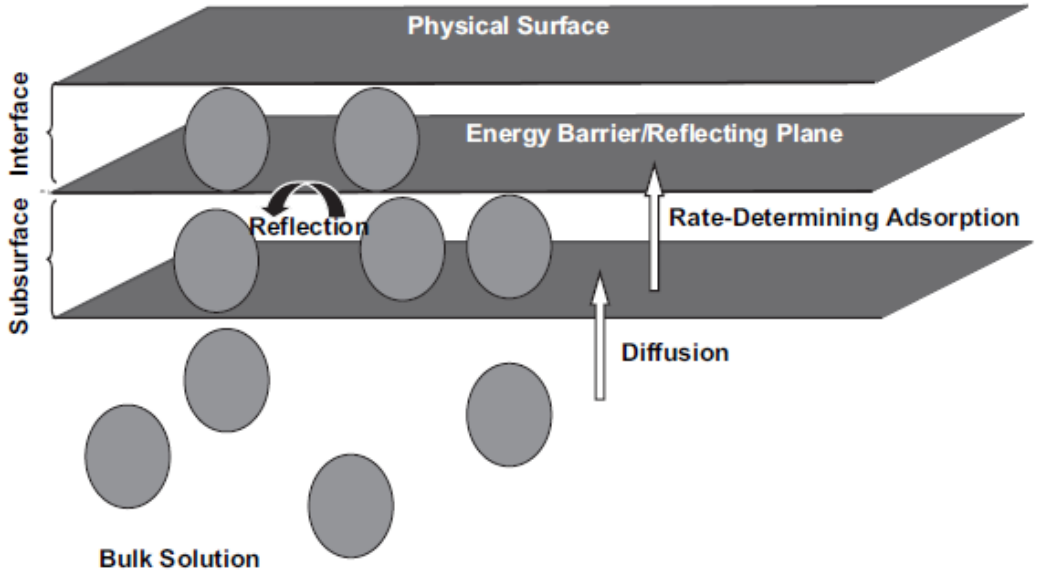

Figure 1-8: Energy Barrier / Reflecting Plane model was developed to bridge the discrepancy between the diffusion theory and measured rates. Taken from [21].

1-10: Protein Adsorption kinetics using solution depletion method and tensiometry

The solution depletion method can be used to measure the concentration of protein in solution before and after contact of the bulk solution with the adsorbent. The change in solution concentration due to adsorption can be calculated by $W_B°$ (initial bulk solution concentration) - W_B (concentration of solution after contact). This change can be referred to as depletion, D (mg/mL) [22]. Figure 1-9 below shows the depletion over time for the protein, Immunoglobulin (IgG). Based on the plot, it can be said with a certain degree of certainty that the depletion in a single protein solution is constant. Figure 2-3 also displays the depletion of IgG at various concentrations –The adsorption kinetics is in

proportion to the bulk concentration. The remainder of proteins, refer to Appendix B, used in the experiment exhibited a similar trend [21].

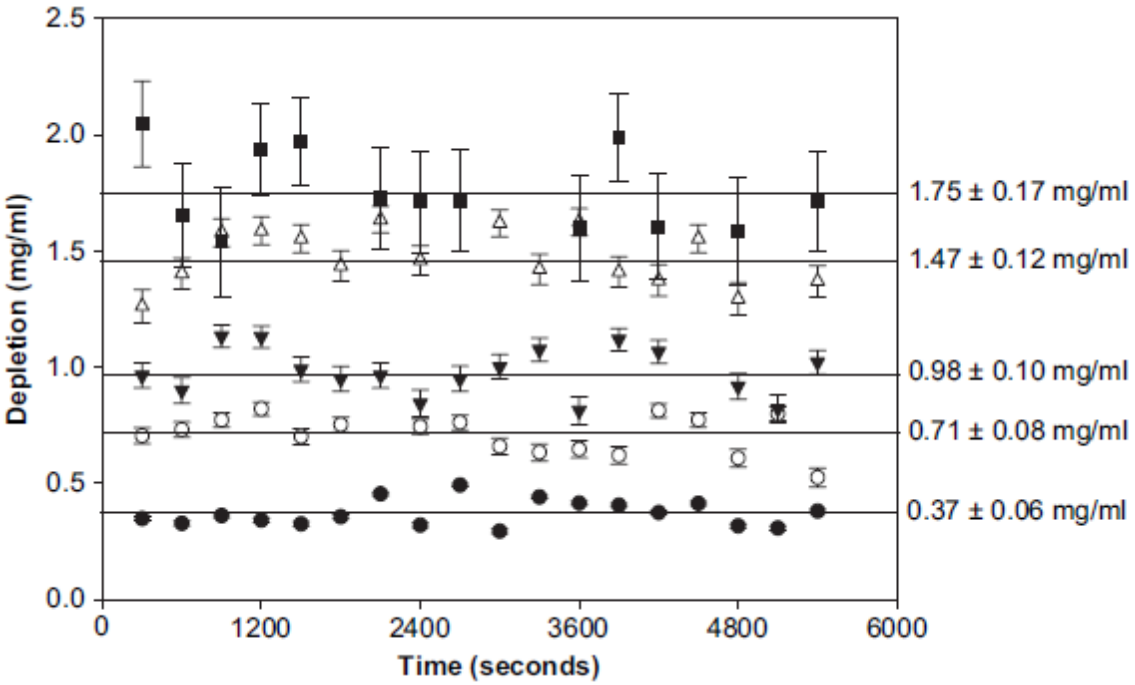

Figure 1-9: Depletion plot for a single protein solution, IgG with varying concentrations - filled circles = 0.8 mg/mL, open circles = 1.6 mg/mL, filled inverted triangles = 2.4 mg/mL, open triangles = 3.2 mg/mL, and filled squares = 3.9 mg/mL. Taken from [21].

Tensiometry utilizes a pendant – drop method to deduce interfacial energies from a pendant-shaped drop via a needle or pipette. The interfacial tensions can subsequently be determined. Figure1-10 shows a 3D (panel A) and 2D (panel B) of the liquid-vapor energetics plotted against the natural logarithm of the bulk concentration. From panel A in Figure 1-10, it can be seen that the energetics are initially at equilibrium. As time progresses, however, there is a rapid decrease and a following formation of a new equilibrium. Panel B shows a decrease in the interfacial tension with increasing natural logarithm of concentration of the bulk solution [21].

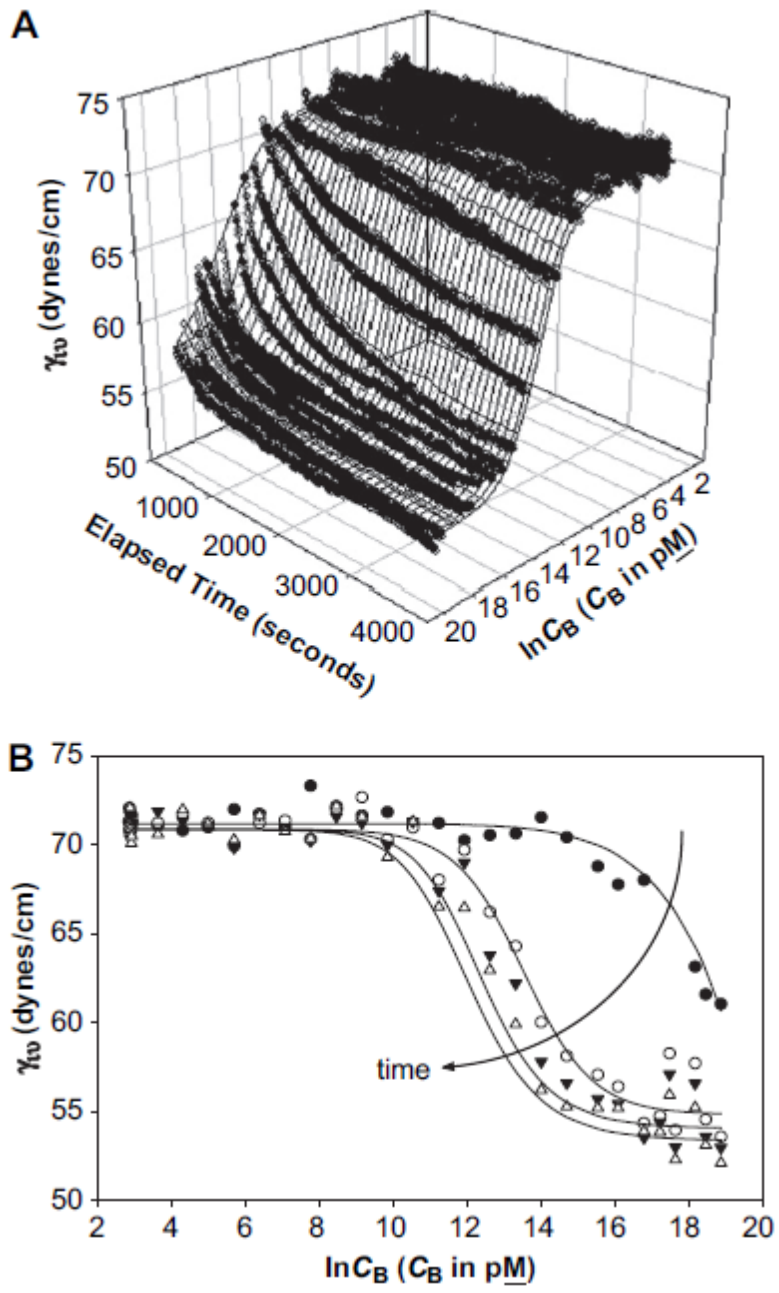

Figure 1-10: Plots of interfacial tension versus concentration. Panel A represents a 3D plot of the interfacial tension versus elapsed time and ln(C_B). Panel B is a plot of interfacial tension versus ln(C_B). Taken from [21].

1-11: Interpretation of the experiments

There are two main observations from the experiments [21]:

(1) The total mass of protein adsorbed to the surface from the bulk solution remained constant in the span of $5 \leq t \leq 90$ min.

(2) The interfacial energetics were dynamic over 0.25 sec $\leq t \leq 60$ min.

These two observations show that mass transfer does not result in the decrease in the interfacial energetics as mass transfer remains constant when the interfacial energetics are changing. According to conventional Gibbsian surface thermodynamics, interfacial tensions decrease because protein concentration within the surface region increases. There are three ways that an interphase concentration can increase:

(1) An increase in the mass of the adsorbate when the interphase volume is fixed

(2) If the interphase volume decreases while the total mass remains constant.

(3) In the situation when (1) and (2) occur simultaneously [17], [21].

Since it known that the mass of the adsorbate is constant, (1) and (3) cannot explain the observations. This leaves (2), which means that the interphase volume must decrease to change the interfacial tension over the specified time interval [21].

Figure 1-11 shows a physical model of the adsorption kinetics in a single-protein solution. At the instant that the bulk solution comes into contact with a physical surface, a thin interphase layer forms (panel A). Then protein molecules move into the interphase region from the bulk solution by displacing the water molecules present in the interphase. This causes the expansion of the interphase (panel B). The interphase then undergoes a

shrinking process by removing the water molecules to achieve a densely packed region (panel C). Finally, the shrinking subsides and an energetically favorable steady state is obtained (panel D) [17], [21].

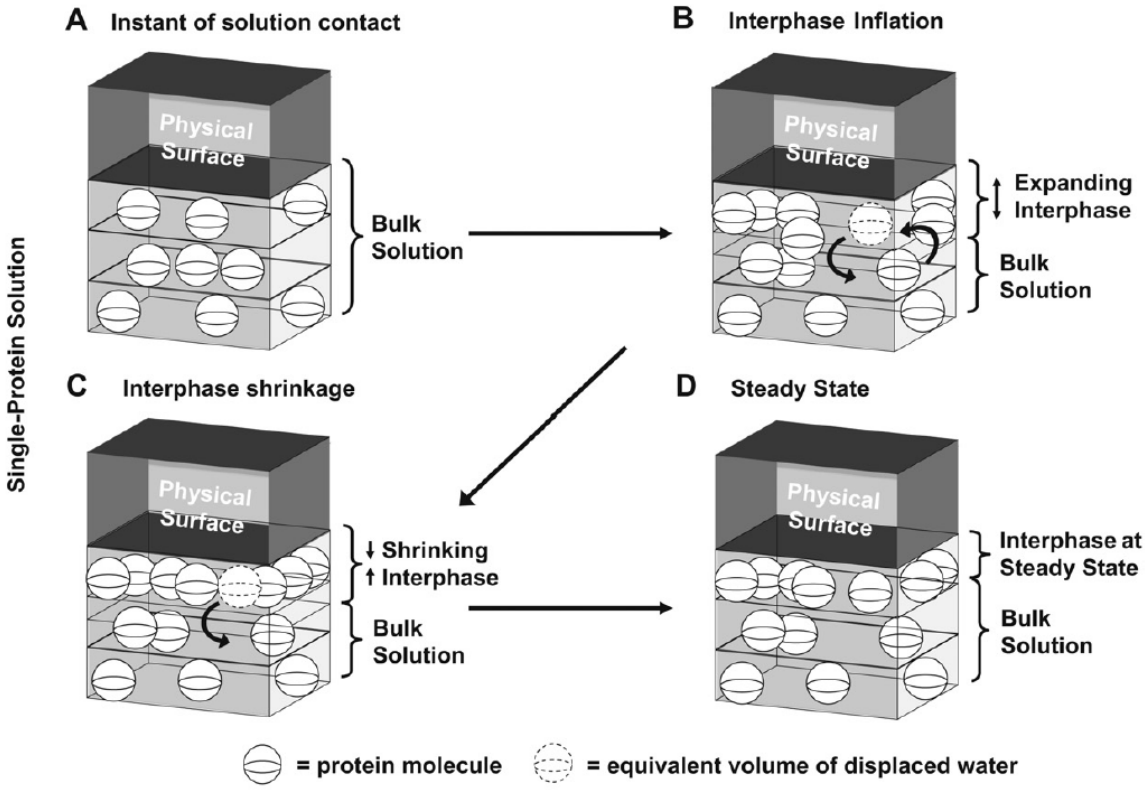

Figure 1-11: Panels A-D show the formation and development of the interphase layer. Taken from [17].

1-12: Binary adsorption competition scenarios

It is unreasonable to conduct experiments using numerous protein combinations at different concentrations. Adsorption competition between two dissimilar sized proteins can be broken down into five distinct cases. These cases correspond to the bulk solution

concentrations of the proteins that are required to saturate the adsorbent surface. The bulk solution concentration of the i^{th} protein is represented by W^{o}_{Bi}, where W indicates bulk solution concentration, *o* indicates initial concentration, and *i* indicates either protein *i* or *j*. The saturating bulk solution concentration is designated by $(W^{o}_{Bi})^{max}$. Finally, the total binary solution concentration is shown by $(W^{o}_{B})_{i,j}$, where "*i,j*" subscript indicates a binary mixture [23].

Case 1: Proteins *i, j* can neither individually nor collectively can saturate the adsorbent surface at the bulk solution concentrations.

Case 2: Proteins *i, j* cannot individually saturate the adsorbent surface but can collectively saturate the surface at bulk solution concentrations.

Case 3: Protein *i* at bulk solution concentration can independently saturate the adsorbent surface, while protein *j* is at a bulk solution concentration that cannot independently saturate the surface.

Case 4: Protein *j* at bulk solution concentration can independently saturate the adsorbent surface, while protein *i* is at a bulk solution concentration that cannot independently saturate the surface.

Case 5: Both proteins *i* and *j* are at bulk solution concentrations that are sufficient to independently saturate the surface.

Using various combinations of the proteins stated in the Appendix C, solution depletion method was used for the each of the above cases. Figure 1-12 represents the full range of competition behaviors observed in experiments summarized in Appendix D. In cases 4 and 5 there are two steady state regions: state 1 and state 2. These steady state

regions are shown in panels A and B in Figure 1-12. Cases 1 and 3, however, did not consistently result in the two steady state regions – see panel C in Figure 1-12.

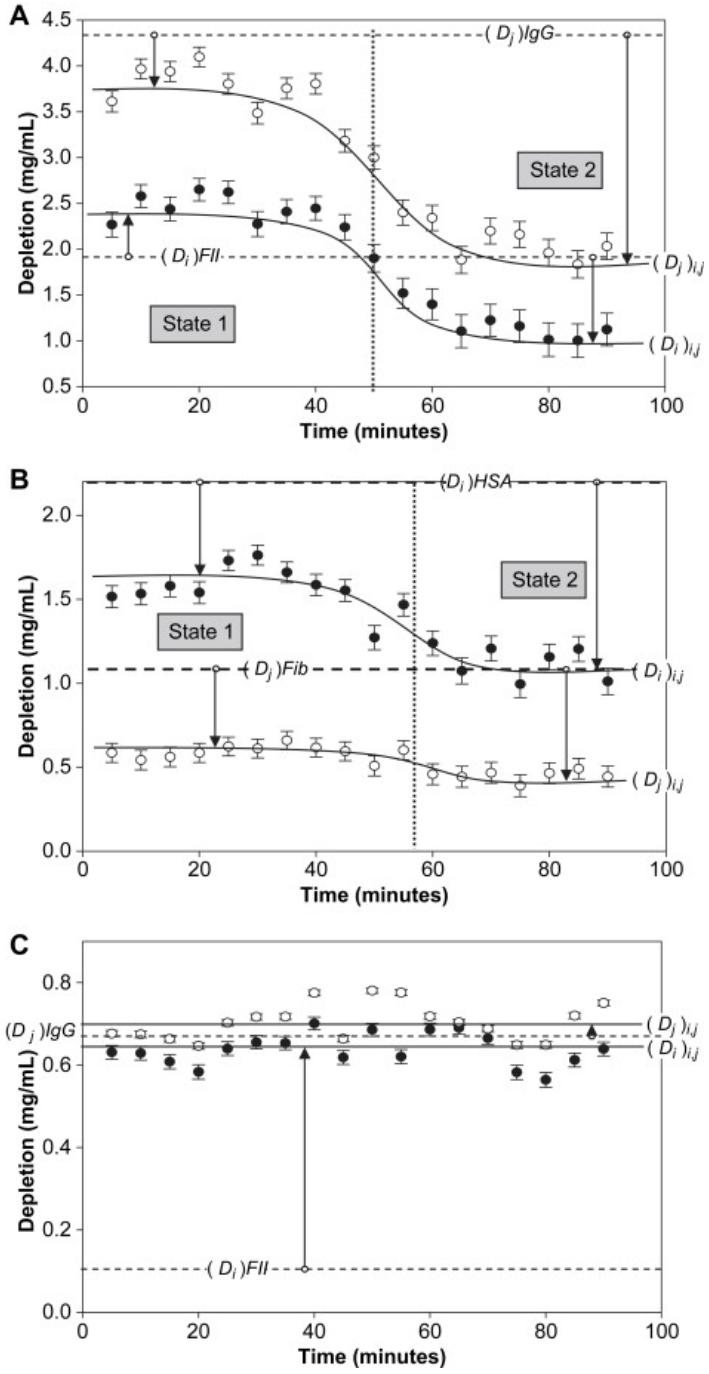

Figure 1-12: Depletion curves indicating state 1 and state 2 for all of the concentration cases in a binary solution. In panels A and B, two states can be seen while in panel C, a single state is shown. Taken from [23].

Figure 1-13 plots the Depletion ratio ($(D_j)_{i,j}/(D_i)_{i,j}$) versus initial bulk solution concentration ratio ($(W^o_{Bj})_{i,j}/(W^o_{Bi})_{i,j}$) for Human Serum Albumin (HSA) and Fibrinogen (Fib) at state 1. It can be seen that there is a bias towards the concentration ratio from the figure below. Thus the slope of the best fit line, defined as S_{ij}, can be interpreted as a selectivity factor. The equation governing the best fit line is $(D_j)_{i,j}/(D_i)_{i,j} = S_{ij}*(W^o_{Bj})_{i,j}/(W^o_{Bi})_{i,j}$. Simply put, the selectivity is the ratio of the depletion ratio to the concentration ratio. Similar to this, S_{ij} for other protein combinations is stated in Appendix D.

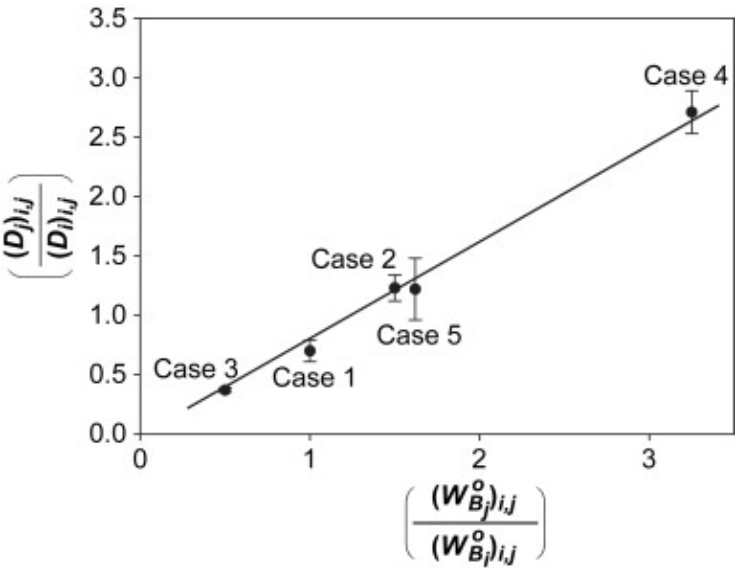

Figure 1-13: When the depletion ration is plotted against the bulk concentration ratio, there is a linear relationship. It can be seen that there is not a one-to-one relationship between the depletion ratio and the bulk concentration ratio. The slope of the linear trend represents the selectivity. Taken from [23].

Though two states were observed, only state 1 was considered. This is because state 1 is transient, while it is unknown whether state 2 is transient. It cannot be stated with certainty that there is not a state 3. But this document assumes that state 2 is the final equilibrium [23].

1-13: Protein adsorption in a binary solution

Adsorption of two or more proteins in solution to the same adsorbent surface follows the general outline of events described for adsorption of a single-protein solution. Figure 1-14 is the corresponding physical model of protein adsorption in a binary solution. At the first instant that the binary solution comes into contact with the physical surface, a thin interphase region is formed similar to that in a single-protein solution (panel A). There is a relative concentration gradient between the interphase and the bulk solution causing protein molecules to diffuse into the interphase thereby increasing the size of the interphase (panel B). Subsequently, the volume of the interphase decreases to make the region more energetically favorable by dispelling water (panel C). Finally, the protein molecules reach steady state (panel D).

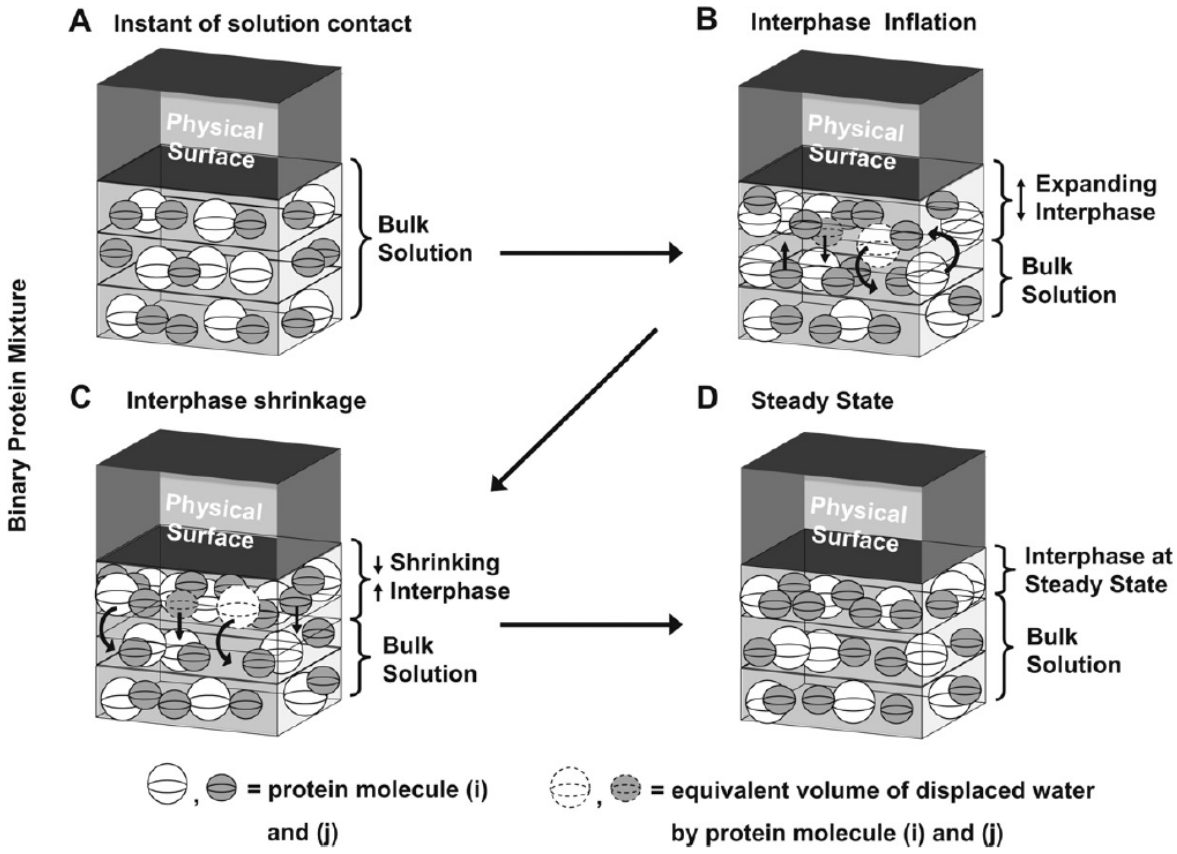

Figure 1-14: Panels A-D show the formation and development of the interphase layer in a binary solution of two dissimilar proteins. The process is similar to that of a single protein solution. Taken from [23].

The major difference between the adsorption in a single-protein solution and a binary solution is protein competition. In a single-protein solution, only a single protein is present and thus the depletion is proportional to the initial bulk concentration of the corresponding protein. In a binary solution, however, there are two proteins that diffuse into the interphase region, resulting in protein competition. This subject matter is still relatively unknown as the defining parameters that govern the competition are not yet determined.

1-14: The Stokes-Einstein-Sutherland (SES) Equation

The Stokes-Einstein-Sutherland (SES) Equation relates the diffusion coefficient (C) to the temperature (T), radius (R), Boltzmann Constant (k_B), and viscosity (η). Refer to Appendix E for a derivation of the SES Equation. Equation (1) below is a form of the SES Equation that will be used in this document [22].

$$C = \frac{k_B T}{6\pi\eta R} \qquad \text{Equation (1)}$$

The diffusion coefficient refers to a specific protein, either the i^{th} or j^{th}. However, understanding the adsorption kinetics of a binary solution is of interest. Thus finding the diffusion coefficient ratio of the j^{th} protein to the i^{th} protein may offer some insight on the parameters that govern protein competition in a binary solution. Assuming a constant temperature and viscosity, the diffusion coefficient ratio becomes a ratio of the two radii. Using the radius to molecular weight relationship described in section 1-6, the ratio of the diffusion coefficients can be related to the molecular weight ratio as shown by Equation (2) [23].

$$\frac{C_j}{C_i} = \left(\frac{MW_j}{MW_i}\right)^{-1/3} \qquad \text{Equation (2)}$$

The diffusion coefficient ratio that has been derived can be approximated as the protein selectivity. In Figure 1-16, the diffusion coefficient ratio and selectivity are plotted against the molecular weight ratio. From the figure, it can be seen that the diffusion coefficient ratio follows the same general trend as the selectivity, which has been obtained from experimental data. The SES Equation over predicts the selectivity at low molecular weight ratios and under predicts the selectivity at high molecular weight ratios. The selectivity plateaus at high molecular weight ratios while the diffusion coefficient ratio continues to decrease. The scope of this paper aims to modify the equation to fit the experimental data. Since only molecular weights and concentrations of proteins are known, the viscosity will be a function of molecular weight and concentration.

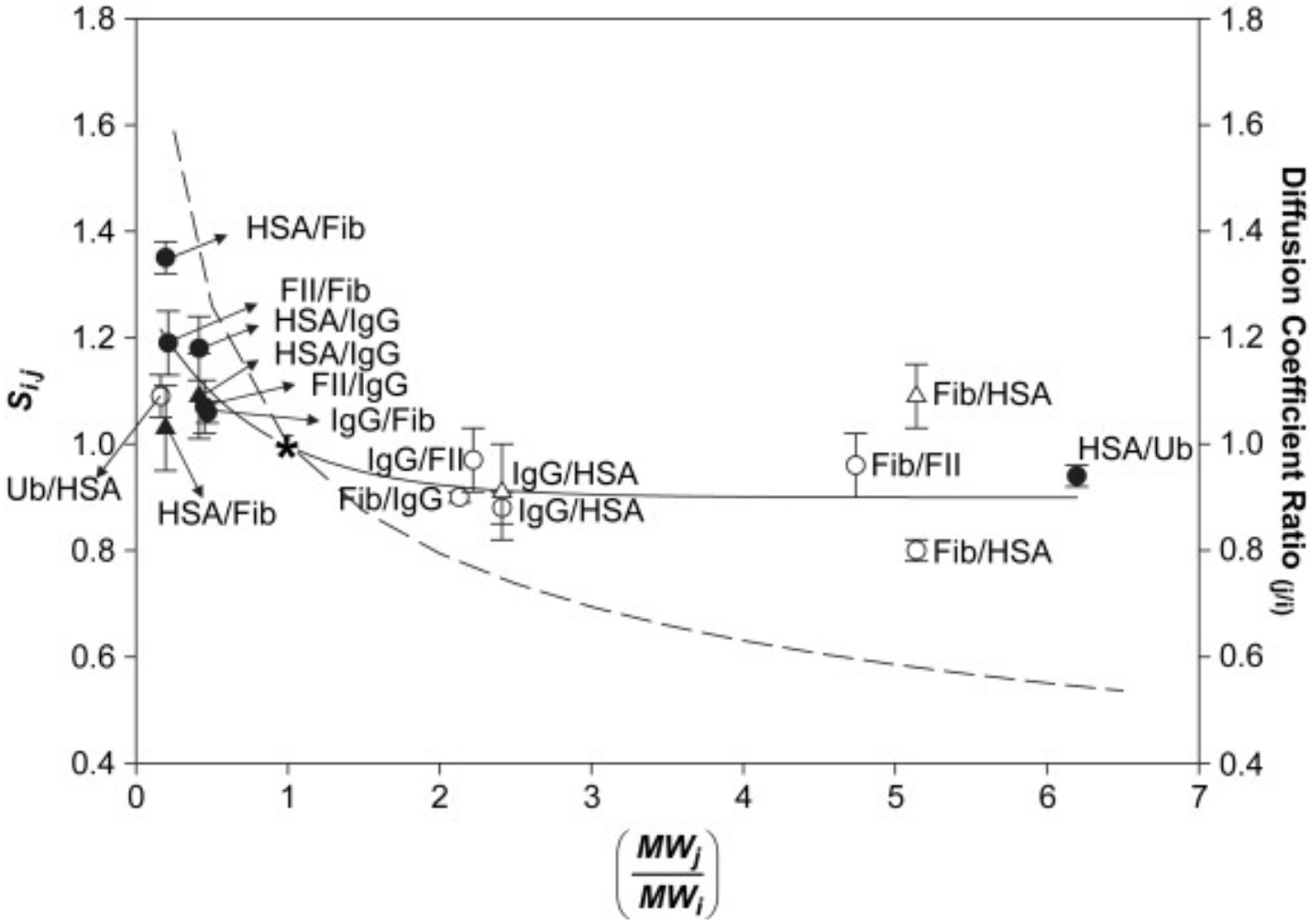

Figure 1-15: Plot of the approximate SES equation and experimental selectivity data against molecular weight ratio. The dashed line represents the SES plot governed by Equation (2). The solid line is drawn to act as a guide for the data. Taken from [23].

1-15: Summary

In this chapter, the literature on protein adsorption was summarized. Initially, adsorption and the interphase region were discussed. This was followed by a discussion on proteins and treating the proteins as spheres. Finally, adsorption of proteins in single solution and binary solution was discussed. In Chapter 2, the project goals, methodology, and results will be discussed. In Chapter 3, a discussion of the results will be presented followed by future directions for the project. In Chapter 4, the conclusion can be found. This is followed by the references and appendices that are referred to in the text.

Chapter 2 : Methods and Results

2-1: Project Goals

In Figure 1-16, there is a discrepancy between the experimental data of selectivity and the diffusion coefficient ratio calculated using Equation (2), which assumes that the viscosity ratio of the proteins to be constant. This project seeks to derive the diffusion coefficient ratio with the assumption that the viscosity ratio is not constant. Since the change in viscosity ratio is not known, the ratio will be determined using various models such as applying viscosity suspension models and using standard equations to perform a trial and error analysis.

2-2: Methods

The diffusion coefficient is defined by Equation (1), K_B is the Boltzmann constant, T is temperature, η is viscosity, and r is the radius.

$$C = \frac{k_B T}{6\pi\eta r}$$

In the case of two dissimilar proteins, i and j, the diffusion coefficients can be defined as

$$C_i = \frac{k_B T}{6\pi\eta_i r_i} \qquad \text{Equation (3)}$$

$$C_j = \frac{k_B T}{6\pi\eta_j r_j} \qquad \text{Equation (4)}$$

The Boltzmann constant and temperature are the same for both proteins, while the viscosity and radius change. Using equations (3) and (4) to find the ratio of the diffusion coefficients of the j^{th} protein relative to the i^{th} protein:

$$\frac{C_j}{C_i} = \frac{\frac{k_B T}{6\pi\eta_j r_j}}{\frac{k_B T}{6\pi\eta_i r_i}}$$

$\frac{C_j}{C_i} = \left(\frac{\eta_i}{\eta_j}\right)\left(\frac{r_i}{r_j}\right)$ Equation (5)

In section 1-6, the relationship between protein radius and molecular weight was defined. The definition can be applied to proteins, *i* and *j*.

$$r_i = 6.72\ X\ 10^{-8}\ (MW_i)^{\frac{1}{3}}$$

$$r_j = 6.72\ X\ 10^{-8}\ \left(MW_j\right)^{\frac{1}{3}}$$

The relations shown above can then be substituted into Equation (6), which then becomes:

$$\frac{C_j}{C_i} = \left(\frac{\eta_i}{\eta_j}\right)\left(\frac{6.72\ X\ 10^{-8}\ (MW_i)^{\frac{1}{3}}}{6.72\ X\ 10^{-8}\ \left(MW_j\right)^{\frac{1}{3}}}\right)$$

$$\frac{C_j}{C_i} = \left(\frac{\eta_i}{\eta_j}\right)\left(\frac{MW_i}{MW_j}\right)^{\frac{1}{3}}$$

$\frac{C_j}{C_i} = \left(\frac{\eta_i}{\eta_j}\right)\left(\frac{MW_j}{MW_i}\right)^{-\frac{1}{3}}$ Equation (6)

If the viscosity ratio,$\frac{\eta_i}{\eta_j}$ is constant Equation (2) from section 1-14 will be derived. As previously discussed, this equation fails to predict a diffusion coefficient ratio that accurately predicts the selectivity of proteins. Thus the viscosity ratio shown in Equation (6) will be modeled using different equations in order to correct the discrepancy shown in Figure.

2-2.1: Data Analysis

After generating an equation, SigmaPlot was used to perform the data analyze. Excel was used for the viscosity suspension models and SigmaPlot was used for fitting the standard equations. This was because the viscosity suspension models were dependent on concentration as well as molecular weight.

For analysis using SigmaPlot, the data found in Appendix D was entered in the cells. Then the generated equation was programmed into the software using the function, "create new equation." The equation was dynamically fitted to the experimental data of mean selectivity. Though the standard deviation is part of the individual data points, it was not part of the actual fit.

The coefficient of determination, R –squared, provides a measure of how well a model predicts the future outcomes. Thus along with qualitative inspection of the fit of the equation, the R-squared value will also be examined. An ideal equation will have R-squared values above 0.7 and a good qualitative fit [25].

2-3: Viscosity Suspension Models

Human blood is a suspension of formed elements such as red blood cells, white blood cells, and platelets in plasma. The viscosity of blood is a function of the hematocrit, which is the percent ratio of the volume of red blood cells relative to the volume of blood. As the number of red blood cells increases, the hematocrit increases, this results in the increase in the blood viscosity. If the number of red blood cells decreases, the blood viscosity will decrease [26].

Blood viscosity also changes with shear rate. Holding the concentration of red blood cells constant, under low shear rates, blood viscosity will increase because the red blood cells will aggregate (rouleaux formation) [27], [28]. At high shear rates, red blood cell aggregates will be broken down resulting in a decrease in the blood viscosity. This theory applies to plasma proteins such as fibrinogen and immunoglobulin [29].

The two primary factors affecting blood viscosity are red blood cell concentration and shear rate. However, many of the early studies of blood viscosity were based only on concentration. Einstein's viscosity model:

$$\eta = \eta_f(1 + 2.5C) \qquad \text{Equation (7)}$$

η = suspension viscosity

η_f = fluid viscosity

C = concentration of red blood cells

Equation (7) is only applicable for a dilute suspension of spheres – that is the concentration must be less than 10% [30]. Hatschek model, represented by Equation (8) was obtained using a rotating viscometer [31], [32].

$$\eta = \eta_f \frac{1}{1-C^{1/3}} \qquad \text{Equation (8)}$$

In a similar manner, Cokelet's model was developed:

$$\eta = \eta_f \frac{1}{(1-C)^{2.5}} \qquad \text{Equation (9)}$$

2-3.1: Results for Einstein

Einstein's viscosity model is dependent on particle concentration and fluid viscosity. However, the model is only accurate for particle concentration up to 10%. Since the protein concentrations used in the experiments are less than 10%, this model is applicable. Einstein's viscosity model is shown in Equation (11).

$$\frac{C_j}{C_i} = ax^{-\frac{1}{3}} * \frac{1+2.5(W_{Bi}^{\circ})_{i,j}}{1+2.5(W_{Bj}^{\circ})_{i,j}} \qquad \text{Equation (10)}$$

$\frac{C_j}{C_i}$ = Diffusion Coefficient Ratio = Selectivity

a = Constant

x = Molecular Weight Ratio = (MWj/MWi)

$(W_{Bi}^{\circ})_{i,j}$ = Concentration of the ith protein

$(W_{Bj}^{\circ})_{i,j}$ = Concentration of the jth protein

The figures below show a qualitative fit of the data using case 1, case 3, and case 5 protein concentrations that were discussed in section 1-12 and Table 2-1 summarizes the r squared values for each case.

Case 1

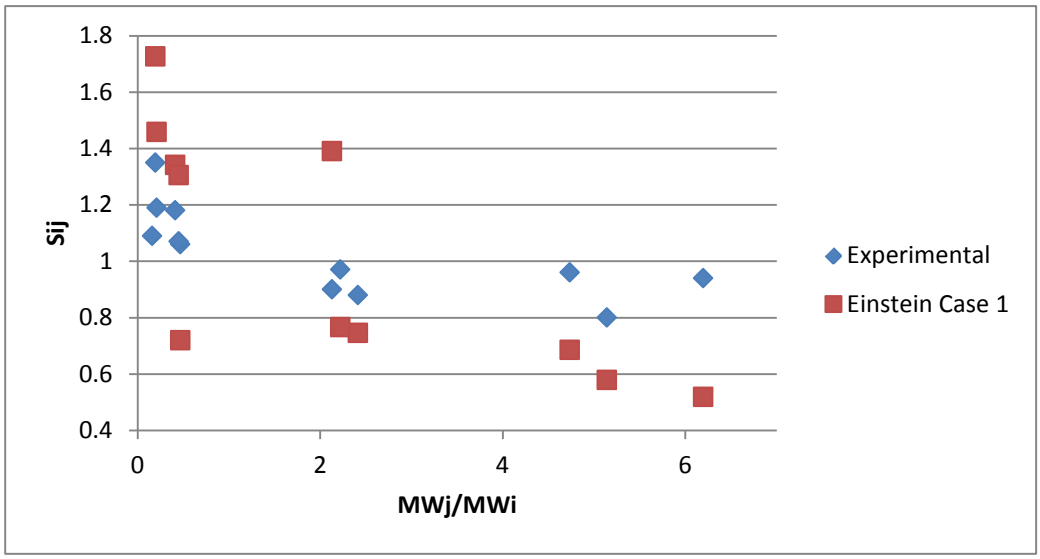

Figure 2-1: Case 1 concentration data of the Einstein Equation qualitatively shows a poor fit. At low molecular weight ratios, the selectivity is over predicted while it is under predicted at high molecular weight ratios.

Case 3

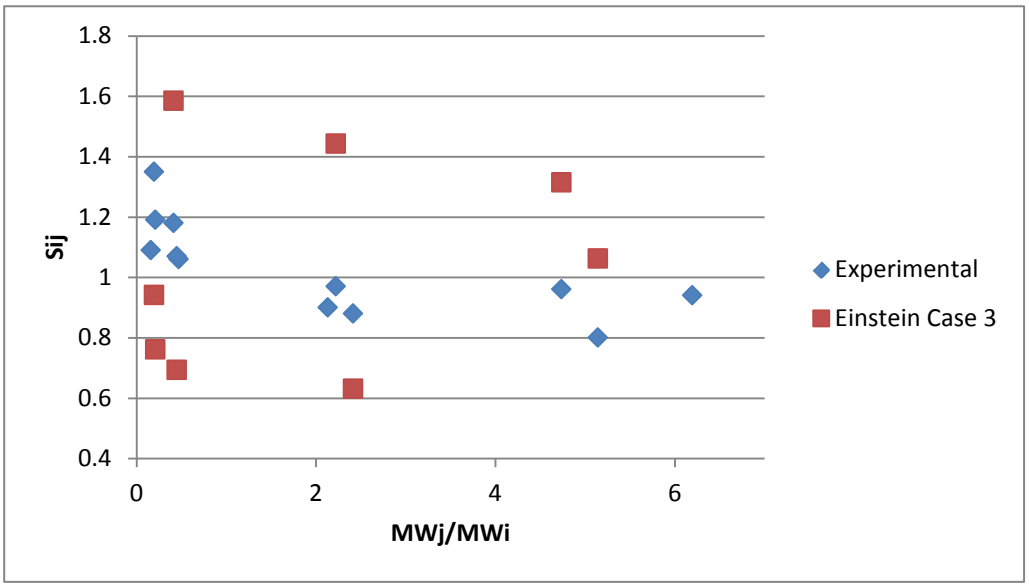

Figure 2-2: Case 3 concentration data of the Einstein Equation does not correlate with the experimental selectivity data. The predicted values do not follow the data.

Case 5

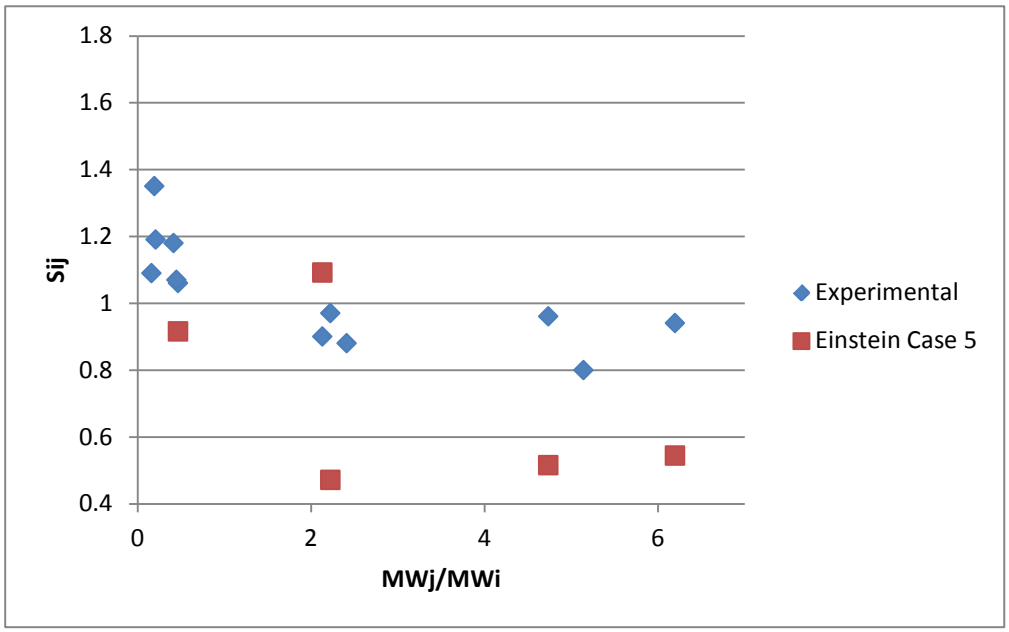

Figure 2-3: Case 5 concentration data of the Einstein Equation did not predict selectivity well. There are only 5 points that fell in the defined axis window. The remaining values were out of the axis window.

Table 2-1: Summarizes the data analysis for the 3 concentration cases for Einstein's equation. The r-squared value was 0 in all three cases implying that there is no correlation with the experimental data.

Case	R	Rsqr	Standard Error of Estimate	a	standard error
1	0	0	0.384	0.9138	0.1038
3	0	0	0.6841	0.4842	0.1178
5	0	0	0.514	0.5691	0.0918

Both the figures and the table indicate that the Einstein's Viscosity Model is not a good fit for the viscosity ratio. The r squared value for each case is 0, which indicates no correlation between the experimental data and Equation (10).

2-3.2: Results for Cokelet's Model

Cokelet's viscosity model is dependent on fluid viscosity and particle concentration. It is applicable for a wider concentration range than Einstein's model. The model is described by Equation (11) below:

$$\frac{C_j}{C_i} = ax^{-\frac{1}{3}} * \left(\frac{1-(W_{Bj}°)_{i,j}}{1-(W_{Bi}°)_{i,j}}\right)^{2.5} \qquad \text{Equation (11)}$$

$\frac{C_j}{C_i}$ = Diffusion Coefficient Ratio = Selectivity

a = Constant

x = Molecular Weight Ratio = (MWj/MWi)

$(W_{Bi}°)_{i,j}$ = Concentration of the ith protein

$(W_{Bj}°)_{i,j}$ = Concentration of the jth protein

In the figures below, the protein concentrations for cases 1, 3, and 5 were used. The data was extracted from the selectivity table found in Appendix D.

Case 1

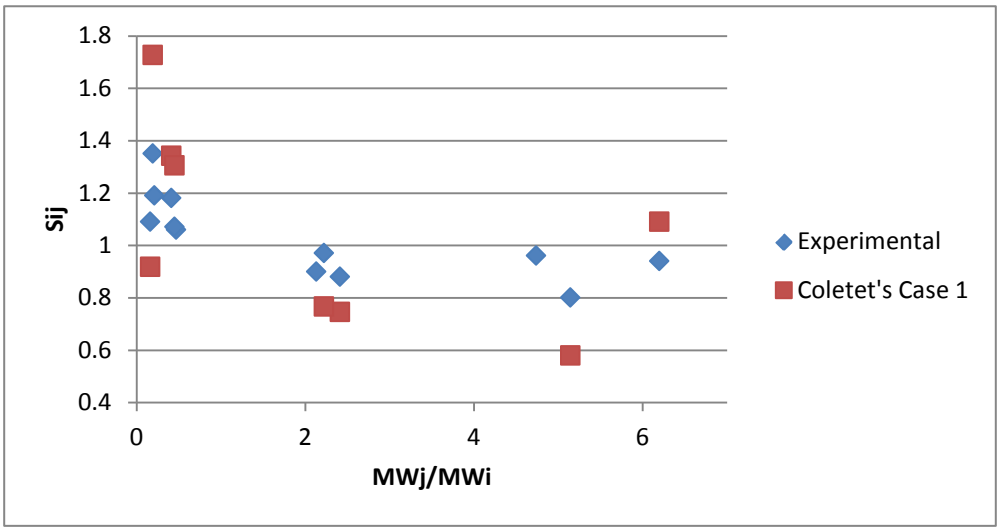

Figure 2-4: Cokelet's viscosity model for case 1 concentration data follows a similar trend to the experimental data.

Case 3

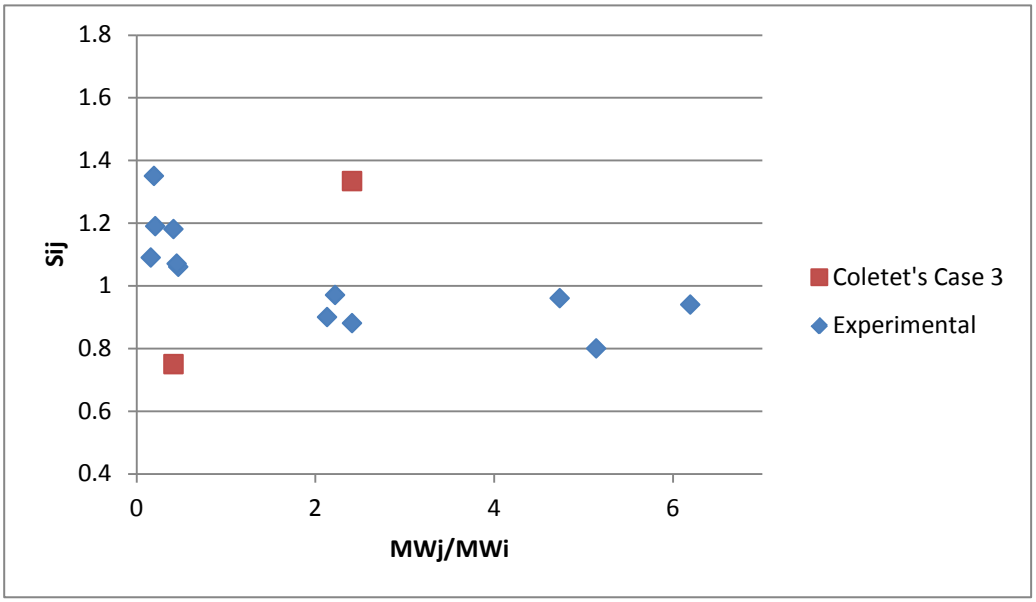

Figure 2-5: Cokelet's viscosity model for case 3 concentration data does not contain enough points in the axis window to determine a trend.

Case 5

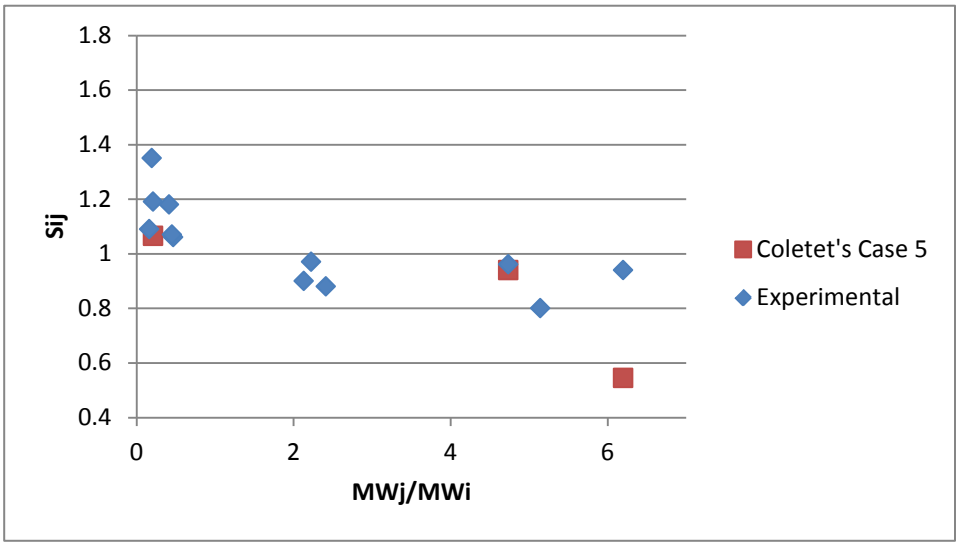

Figure 2-6: Cokelet's viscosity model for case 5 concentration data does not contain enough points in the axis window to determine a trend.

Table 2-2: Summarizes the data analysis for the 3 concentration cases for Cokelet's viscosity model. The r-squared value was 0 in all three cases implying that there is no correlation with the experimental data.

Case	R	Rsqr	Standard Error of Estimate	a	standard error
1	0	0	0.9889	0.0358	0.0233
3	0	0	0.9372	0.015	0.0076
5	0	0	0.9023	0.1717	0.0765

From Figures 2-4 through 2-6, it can be seen that cases 3 and 5 are not very good fits as most of the data was unable to fit in the selected x and y axis scale bars. The trend does not correspond with that of the selectivity data. The plot of case 1 represented by Figure 2-4 follows the experimental trend. However, statistical analysis done using SigmaPlot resulted in a 0 r squared value. Thus the Cokelet's model is not applicable.

2-3.3: Results for Hatschek

Hatschek's viscosity is also a function of both particle concentration and liquid viscosity. In the figures below, particle concentration corresponding to cases 1, 3, and 5 substituted into Equation (12) below and the diffusion ratio was then plotted.

$$\frac{C_j}{C_i} = ax^{-\frac{1}{3}} * \frac{1-((W_{Bj}°)_{i,j})^{1/3}}{1-((W_{Bi}°)_{i,j})^{1/3}} \qquad \text{Equation (12)}$$

$\frac{C_j}{C_i}$ = Diffusion Ratio = Selectivity

a = Constant

x = Molecular Weight Ratio = (MWj/MWi)

$(W_{Bi}°)_{i,j}$ = Concentration of the i^{th} protein

$(W_{Bj}°)_{i,j}$ = Concentration of the j[th] protein

Case 1

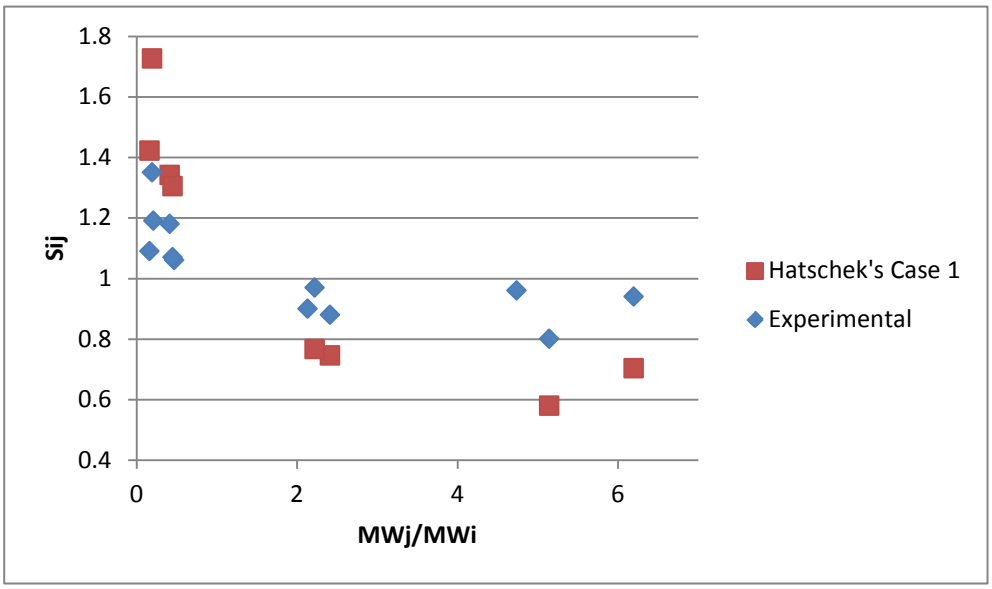

Figure 2-7: Hatschek's viscosity model using case 1 concentration data follows a similar trend to that of the experimental data. The model under predicts the selectivity at low molecular weights though.

Case 3

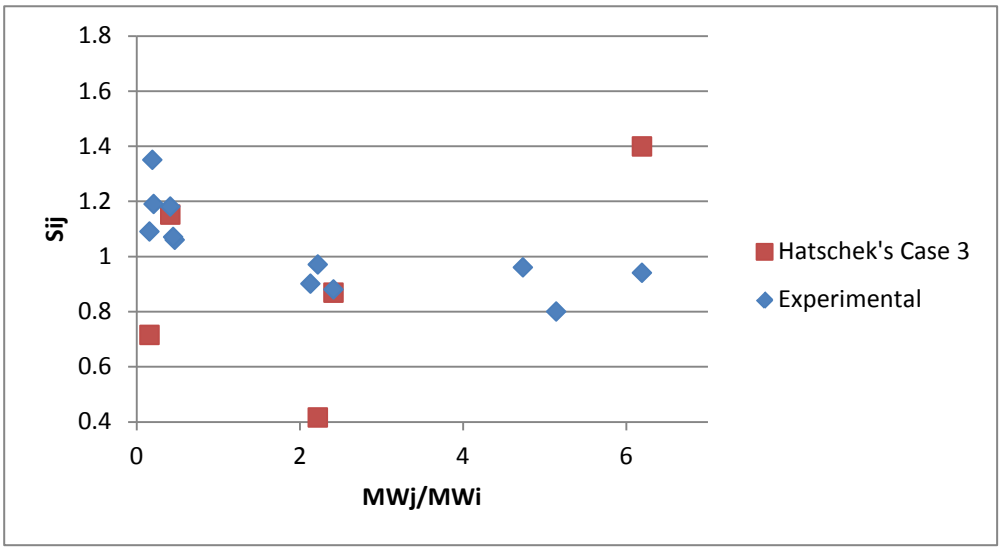

Figure 2-8: Hatschek's viscosity model using case 3 data does not predict enough data points within the defined axis window to draw a correlation.

Case 5

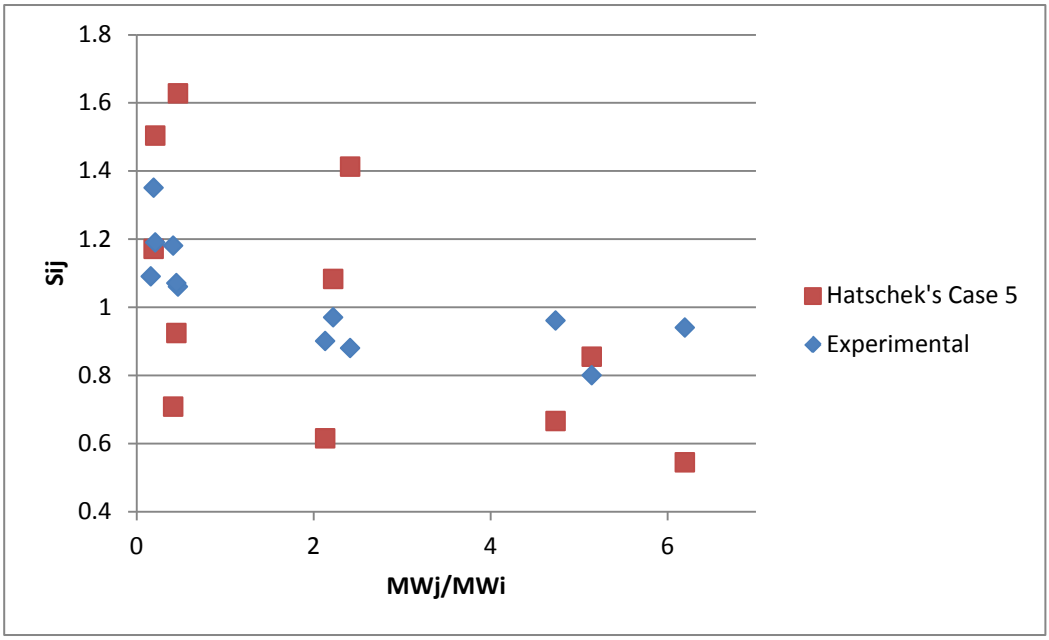

Figure 2-9: Hatschek's viscosity model for case 5 concentration data does not show a trend. The selectivity increases and decreases with increasing molecular weight ratios.

Table 2-3: Summarizes the data analysis for the 3 concentration cases for Hatschek's viscosity model. The r-squared value was 0 in all three cases implying that there is no correlation with the experimental data.

Case	R	Rsqr	Standard Error of Estimate	a	standard error
1	0	0	0.6201	0.4951	0.1033
3	0	0	0.6483	0.3814	0.0851
5	0	0	0.5151	1.1446	0.1852

From a qualitative inspection of Figures 2-7 through 2-9, it can be seen only Figure 2-7 follows a similar trend to the experimental data. Case 1 is similar to the failure of Figure 1-16 in that both follow a similar trend but under predicts the selectivity at high molecular weight ratios. Case 3 does not have enough data points to indicate a trend. This is because the values obtained from Equation (12) for case 3 are too high to fit in the selected axis window. Case 5 indicates an overall decreasing trend but fails to follow the experimental data. From Table 2-3, it can be seen that all of the cases have an r squared value of 0 and thus Hatschek's viscosity model cannot be used to model viscosity.

2-4: Integration of standard equations to viscosity

In the bulk solution, the viscosity for both the i^{th} and j^{th} protein is equivalent. At the interphase, however, the viscosity increases. It is unknown which equation adequately models the trend at which viscosity changes. Thus an approach that can be used is using the standard equations to model the ratio of the viscosities and then see how the SES curve has been modified.

Viscosity was treated strictly as a function of the molecular weight. With that as reference, various equations were generated. Initially, the most fundamental equation:

$y = ax + b$ Equation (13)

y = viscosity ratio

x = molecular weight ratio

a = constant

b = constant

When Equation (13) is substituted into Equation (6) for the viscosity ratio, Equation (14) is obtained. Table 2-4 summarizes the statistics regarding the fit of the equation and Figure 2-10 shows the plot of the equation against the molecular weight ratio.

$$\frac{C_j}{C_i} = ax^{-\frac{4}{3}} + bx^{-\frac{1}{3}} \qquad \text{Equation (14)}$$

$\frac{C_j}{C_i}$ = Diffusion Ratio = Selectivity

x = Molecular Weight Ratio

a = constant

b = constant

Table 2-4: In the data analysis for Equation (14), it can be seen that the r-squared value is 0. This shows that there is no correlation between the predicted selectivity and experimental selectivity.

R	0
Rsqr	0
Standard Error of Estimate	0.1736
a	-0.1017
b	1.2099

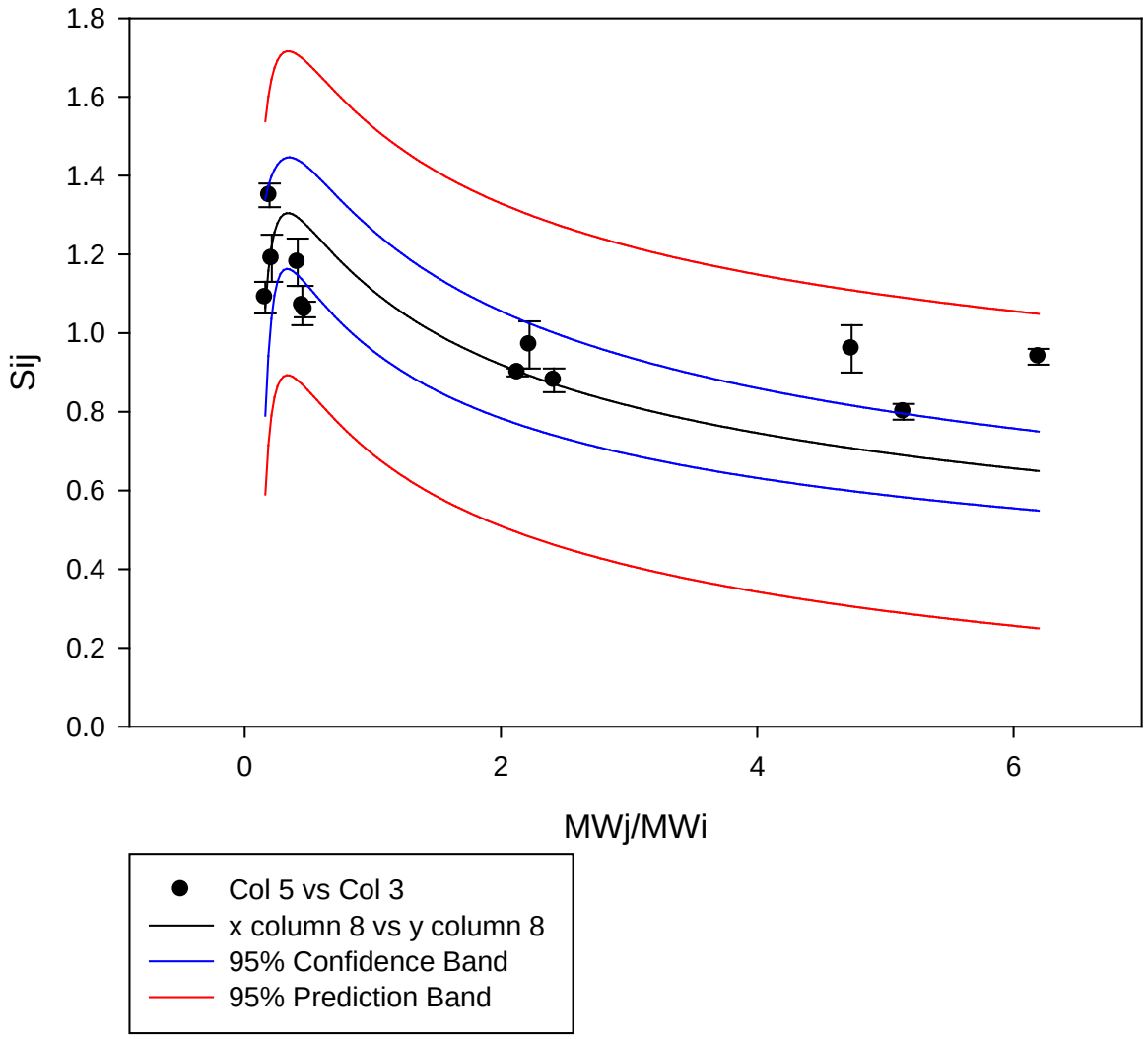

Figure 2-10: In the plot of Equation (14), there is an increase in the selectivity at low molecular weight ratios. The predicted selectivity decreases and eventually under predicts the data.

The equation does not fit the equation as exemplified by Figure 2-10 and the r-squared value found in Table 2-4 indicates no correlation. Thus a linear equation can be eliminated as a potential correction. It is reasonable to assume that polynomial functions will not satisfy the data as they experience an upward trend in the selectivity for low molecular weight ratios.

Using the insight drawn from the analysis of Equation (14), an exponential function was considered.

$y = ae^{-x} + b$ Equation (15)

y = viscosity ratio

x = molecular weight ratio

a = constant

b = constant

Plugging Equation (15) into Equation (6) yields Equation (16) below:

$\frac{C_j}{C_i} = ae^{-x}x^{-\frac{1}{3}} + bx^{-\frac{1}{3}}$ Equation (16)

$\frac{C_j}{C_i}$ = Diffusion Ratio = Selectivity

x = Molecular Weight Ratio

a = constant

b = constant

Table 2-5: The data analysis for Equation (16) shows that the r-squared value is 0.5307. This indicates that the equation fits the data but the fit is simply not good enough.

R	0.7285
Rsqr	0.5307
Standard Error of Estimate	0.1116
a	-0.8652
b	1.4023

Figure 2-11 shows that Equation (16) is good for low molecular weight ratios. But as the molecular weight ratio increases, the selectivity decreases while that of the data shows a steady trend at high molecular weight ratios. From Table 2-5, the r squared value is 0.5307, which is a decent fit to the curve. However, due to unsatisfactory qualitative results, Equation (16) is not the ideal equation to be used.

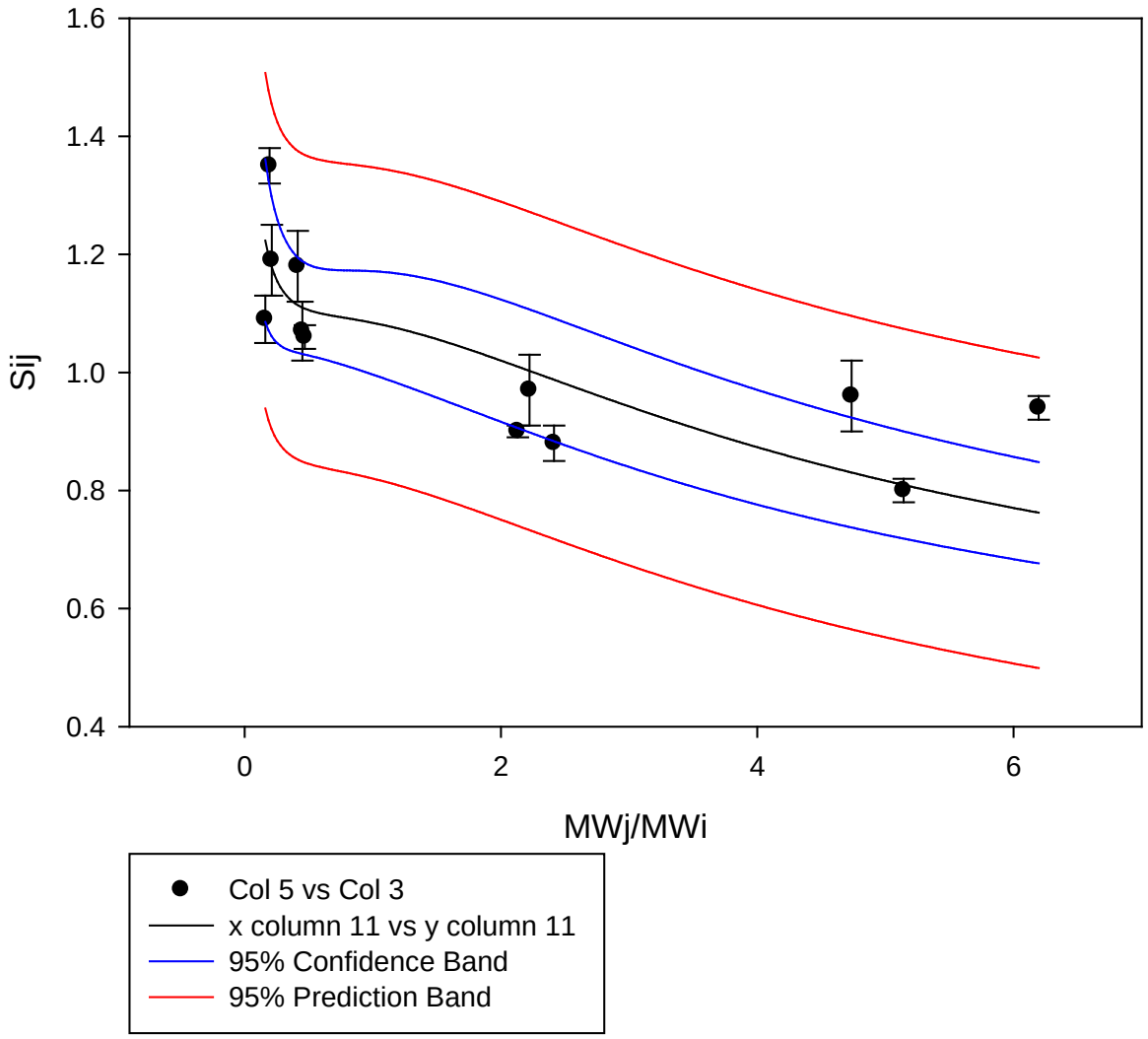

Figure 2-11: The plot of Equation (16) predicts the experimental selectivity at low molecular weight ratios well. But the equation experiences a decreasing trend at high molecular weight ratios and eventually it under predicts the selectivity.

Due to the decent fit of Equation (16), the exponential function can still be considered. The equation must be able to stabilize the curve at higher molecular weights. Thus the difference of incorporating a constant to the exponential term was looked at:

$y = ae^{-x+b} + c$ Equation (17)

y = viscosity ratio

x = molecular weight ratio

a = constant

b = constant

c = constant

Substituting Equation (17) into Equation (6) to obtain Equation (18)

$$\frac{C_j}{C_i} = ae^{-x+b}x^{-\frac{1}{3}} + bx^{-\frac{1}{3}} \qquad \text{Equation (18)}$$

$\frac{C_j}{C_i}$ = Diffusion Ratio = Selectivity

x = Molecular Weight Ratio

a = constant

b = constant

Table 2-6: The data analysis of Equation (18) shows that the r-squared value is 0.5307. This is the same as the analysis of Equation (16). The addition of a constant b to the exponential component did not affect the analysis.

R	0.7285
Rsqr	0.5307
Standard Error of Estimate	0.1116
a	-0.2129
b	1.4023

Equation (18) yielded identical results to Equation (16) as shown by Table 2-6 and Figure 2-12. Since there was not any noticeable difference from a qualitative stand point, Equation (18) was not further pursued.

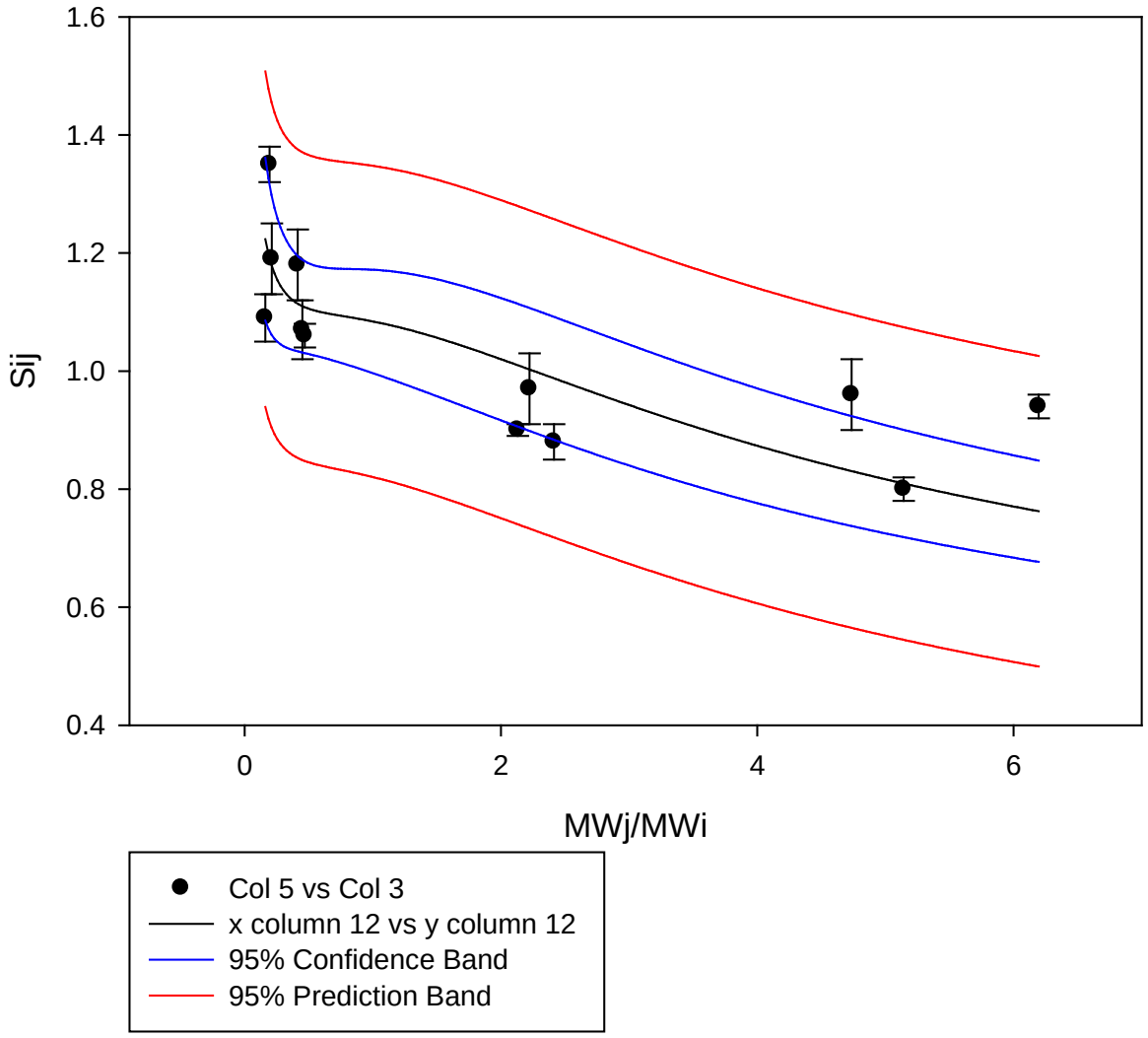

Figure 2-12: The plot of Equation (18) is identical to that of Equation (16). It can be said that the addition of constant b did not positively contribute to the predicted selectivity.

Both Equations (16) and (18) showed that the exponential function is a good for low molecular weight ratios. But the equation must be approximately constant for high molecular weight ratios. Equation (16) and (18) failed to achieve this task due to the molecular weight ratio associated with the constant b. This term caused the further decrease at high molecular weight ratios. If the constant b was eliminated from Equation (18), the equation below was obtained:

$\frac{C_j}{C_i} = ae^{-x}x^{-\frac{1}{3}}$ Equation (19)

$\frac{C_j}{C_i}$ = Diffusion Ratio = Selectivity

x = Molecular Weight Ratio

a = constant

Table 2-7: The data analysis of Equation (19) shows that the r-squared value is 0. This indicates that Equation (19) does not correlate with the selectivity data obtained from the experiments.

R	0
Rsqr	0
Standard Error of Estimate	0.7063
a	0.5396

From Table 2-7 and Figure 2-13, it can quickly be proven that the fit is poor. The key conclusion from Equation (19) is that selectivity remained constant for high molecular weight ratios. The equation was shifted down by some constant.

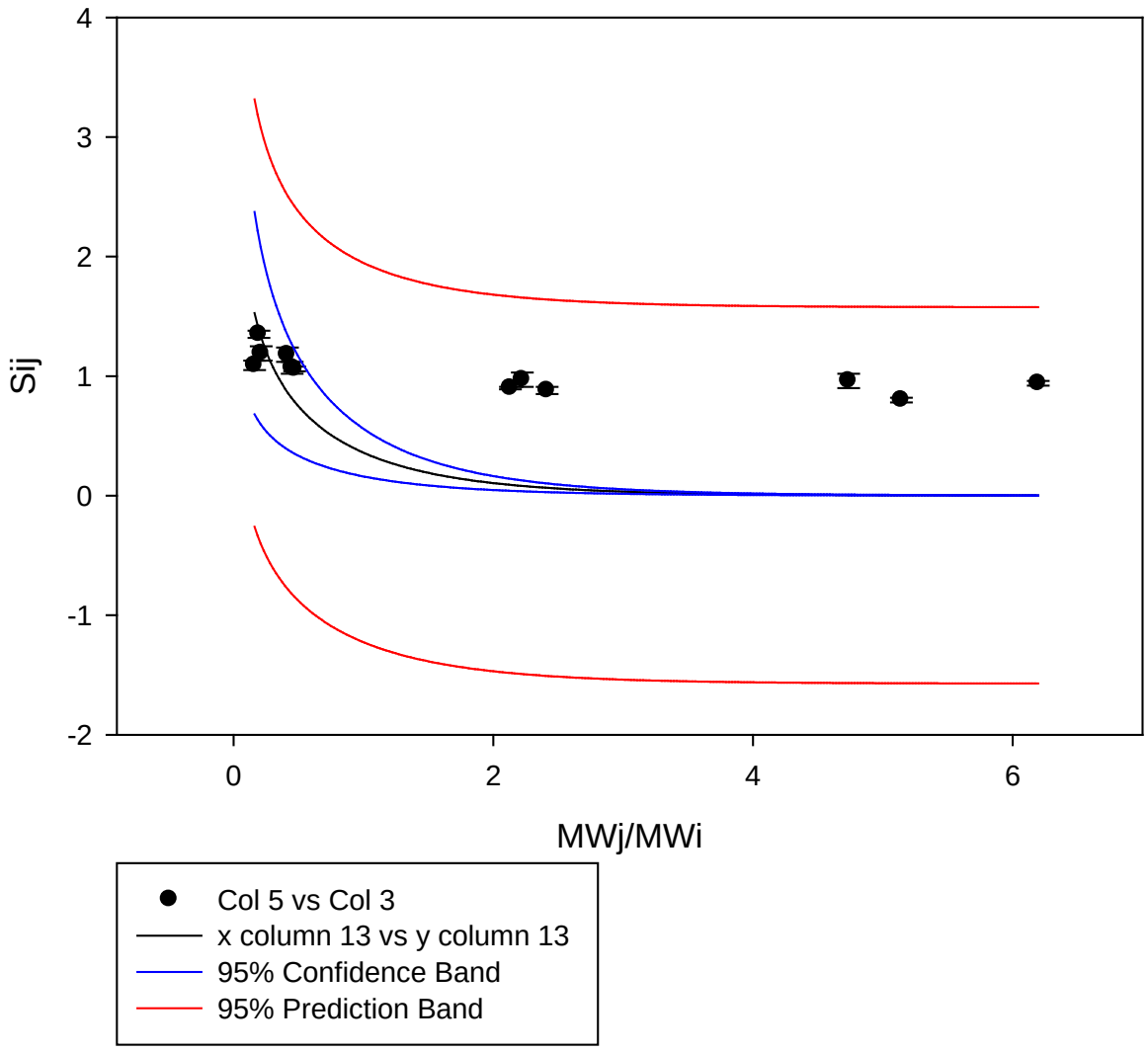

Figure 2-13: Equation (19) does not follow the experimental data. But it does reach a plateau at high molecular weight ratios. Also the entire graph is shifted down by a constant.

Following the analysis for Equation (19), a constant has been added to arrive at the equation below:

$$\frac{C_j}{C_i} = ae^{-x}x^{-\frac{1}{3}} + b \qquad \text{Equation (20)}$$

Table 2-8: The data analysis of Equation (20) shows a very good correlation with an r-squared value of 0.7376. It is above the desired r-squared value of 0.70.

R	0.8588
Rsqr	0.7376
Standard Error of Estimate	0.0835
a	0.087
b	0.9049

The r-squared value from Table 2-8 is 0.7376, which symbolizes a decent fit. Figure 2-14 shows that qualitatively, Equation (20) fits the data. Since Equation (20) models the experimental data both qualitatively and quantitatively, it is assumed to be the correct form of the SES Equation.

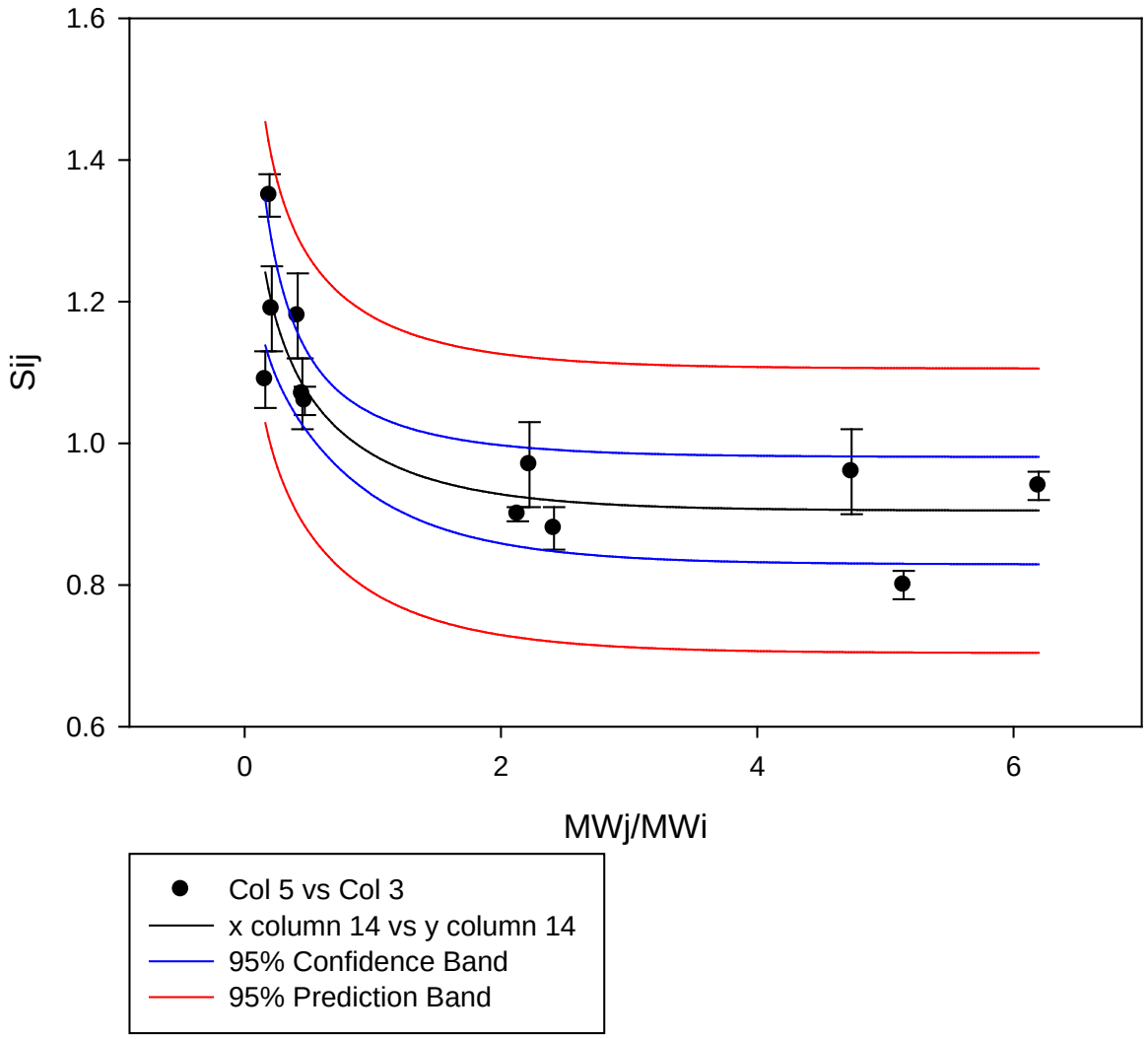

Figure 2-14: The plot of Equation (20) follows the experimental data at both low and high molecular weight ratios.

Chapter 3 : Discussion and Future Directions

3.1: Comparison of the models

The general form of the Stokes-Einstein-Sutherland Equation is $C = \frac{k_B T}{6\pi\eta R}$. If the ratio of C_j to C_i is found, the equation simplifies to $\frac{C_j}{C_i} = \left(\frac{\eta_i}{\eta_j}\right)\left(\frac{r_i}{r_j}\right) = \left(\frac{\eta_i}{\eta_j}\right)\left(\frac{MW_j}{MW_i}\right)^{-\frac{1}{3}}$. In the Biomaterials publication: Volumetric Interpretation of Protein Adsorption: Kinetics of Protein Adsorption Competition from Binary Solution, it was assumed that the viscosity ratio is constant. As a result, only the molecular weight ratio remained in the equation. As shown by Figure 1-16, the diffusion coefficient ratio follows the same trend as the experimental data of selectivity when plotted against the molecular weight ratio. Though the trend is similar, the equation over predicts the selectivity at low molecular weight ratios and under predicts the selectivity at high molecular weight ratios.

Due to the failure of the negative cube root of molecular weight ratio, it can be concluded that the viscosity ratio cannot be treated as constant. Physically, the protein molecules compete to reach the interphase. This competition leads to the formation of a crowding effect near the interphase. Thus it can be assumed that the viscosity ratio is variable at the interphase. However, it is unknown how the viscosity ratio will be changing. Based on the principles governing the Gedanken Model, it is known that the adsorption competition between two dissimilar proteins is dependent on protein size – refer to section 1-8 for a discussion of the Gedanken Model. Experimental data found in Appendix D shows that protein concentration plays a role in determining the adsorption kinetics of two dissimilar proteins. Thus the viscosity is assumed to be a function of concentration and molecular weight.

In the viscosity suspension models, suspension viscosity is a function of strictly particle concentration and liquid viscosity. Since concentration is a factor in determining the selectivity of protein adsorption, the viscosity suspension equations were used for modeling. In Table 3-1 below, results for the Einstein's viscosity equation, Cokelet's viscosity equation, and Hatschek's viscosity equation are summarized. The case number refers to the protein concentration as described by section 1-12. It can be observed that none of the equations fit the data well due to the poor r squared values.

Table 3-1: The viscosity suspension models yielded an r-squared value of 0 for all cases. This shows that the models did not correlate with the experimental data.

Equation	Case	R	Rsqr	Coefficient	Fitted Equation
Einstein	1	0	0	0.9138	$\frac{C_j}{C_i} = ax^{-\frac{1}{3}} * \frac{1 + 2.5(W_{Bi}°)_{i,j}}{1 + 2.5(W_{Bj}°)_{i,j}}$
	3	0	0	0.4842	
	5	0	0	0.5691	
Cokelet	1	0	0	0.0358	$\frac{C_j}{C_i} = ax^{-\frac{1}{3}} * (\frac{1 - (W_{Bj}°)_{i,j}}{1 - (W_{Bi}°)_{i,j}})^{2.5}$
	3	0	0	0.015	
	5	0	0	0.1717	
Hatschek	1	0	0	0.4951	$\frac{C_j}{C_i} = ax^{-\frac{1}{3}} * \frac{1 - ((W_{Bj}°)_{i,j})^{1/3}}{1 - ((W_{Bi}°)_{i,j})^{1/3}}$
	3	0	0	0.3814	
	5	0	0	1.1446	

Since the suspension models were unable to correct the equation, a different approach was taken. The viscosity was treated as strictly a function of molecular weight and equations were generated based on trial and error. Initially, the standard linear equation: y = a*x+ b was used to model viscosity. However, the equation proved to be a poor fit due to the initial rise in selectivity for low molecular weight ratios. Then an exponential function: $y = a*e^{-x} + b$ was modeled. This equation, too failed to satisfy the data despite the decent r value. The main problem with this equation was the decreasing selectivity with increasing molecular weight ratios. Thus the b term was eliminated from the guess and despite a poor fit to the equation, the trend was identical to the experimental data. The curve was shift down by some constant. To the selectivity equation, a constant, b, was added and the equation fit the data both from a qualitative analysis and the

quantitative analysis via the r squared value. So it can be concluded that Equation (20), is the correct version of the Stokes-Einstein-Sutherland Equation.

Physically, Equation (20) implies that the viscosity of the i^{th} protein increases with respect to the j^{th} protein with increasing molecular weight ratios. The molecular weight ratio represents the ratio of the j^{th} protein to the i^{th} protein. An increase in the molecular weight ratio means that there is an increase in the size of the j^{th} protein relative to the i^{th} protein. If the Gedanken model is applied using only the i^{th} and j^{th} protein. For higher molecular weight ratios, where the j^{th} protein is larger than the i^{th} protein, one can expect to see a greater number of i^{th} protein molecules. So it is reasonable to expect the viscosity ratio, modeled by Equation (20), to increase.

3.2: Validation of results using viscometry

The equation that successfully corrected the Stokes-Einstein-Sutherland Equation was derived essentially by a trial and error method. However, the insight gained with the failure of each equation to adequately satisfy the experimental data aided in making the subsequent guess. Also the obtained r-squared valuesfrom SigmaPlot are questionable. A few of the r-squared values were 0, but the fits appear to look decent from a qualitative inspection. Thus, the r-squared values must be validated using a different software program.

To validate the obtained result experimentally, the viscosities of each protein must be measured as a function of concentration. With the knowledge of the viscosities, the corresponding viscosity can be substituted in the modified equation and the diffusion ratio can be found. A viscometer is used to measure the viscosity of a protein. In section 3.2.1 that follows, the different viscometers are discussed.

3.2.1: Viscometers

A capillary viscometer measures viscosity by measuring the time that it takes for the fluid to flow through the capillary. It utilizes the Poiseuille flow relationship and its corresponding assumptions such as: Newtonian Fluid, incompressible flow, rigid circular tube, steady flow, axisymmetric, laminar flow, negligible gravity and uniform flow. Beginning with the Navier – Stokes Equations and using the Poiseuille flow assumptions, the flow rate can be approximated as [33]:

$$Q = \frac{\Delta P \pi R^4}{8 \mu L} \qquad (21)$$

ΔP = Pressure Difference

R = Radius of the pipe

L = Pipe length

μ = Fluid viscosity

The radius and pipe length are known values and if the flow rate and pressure gradient can be determined, the flow rate equation above can be rearranged to obtain viscosity:

$$\mu = \frac{\Delta P \pi R^4}{8 Q L} \qquad (22)$$

Using a force balance between the force due to the pressure and the shear force, the shear stress and wall shear stress can be related to the pressure gradient. Since a Newtonian fluid is involved, the shear stress is linearly proportional to the shear rate.

$$\tau = -\mu \frac{du}{dr} \qquad \text{Equation (23)}$$

Using Equation (23), the following relationships can be drawn:

$$\dot{\gamma}_w = \frac{\Delta P R}{2 \mu L} = \frac{4Q}{\pi R^3} \qquad \text{Equation (24)}$$

Looking at the equations above, it can be seen that shear stress is not constant across the tube. The shear stress would be high near the wall and almost zero at the center, thereby implying that the viscosity is dependent on the shear rate.

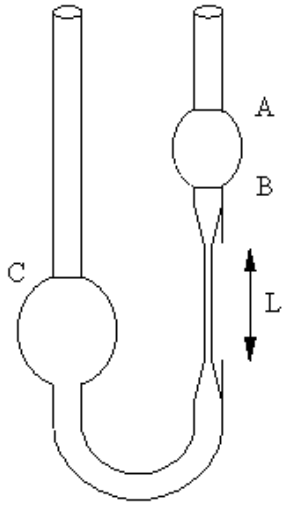

Figure 3-1: The capillary viscometer measures viscosity by taking time measurements of the fluid flow through the pipe. Taken from [34].

The coaxial cylinder viscometer is a type of rotational viscometer. It is typically used to analyze the rheological characteristics of non-Newtonian fluids. The viscosity of a sample of fluid can be found at different shear rates. In the figure below, a coaxial cylinder viscometer is shown. The viscometer contains two cylinders, inner cylinder with a radius of R_1 and an outer cylinder with a radius of R_2, that are called "bob" and "cup", respectfully. The" cup" contains the fluid of interest and is rotated at a constant speed, Ω (rad/sec), while the "bob" remains stationary. The resultant torque, T (dyne-cm), is measured by the angular deflection of the inner cylinder. In the figure below, a coaxial cylinder viscometer is shown [33].

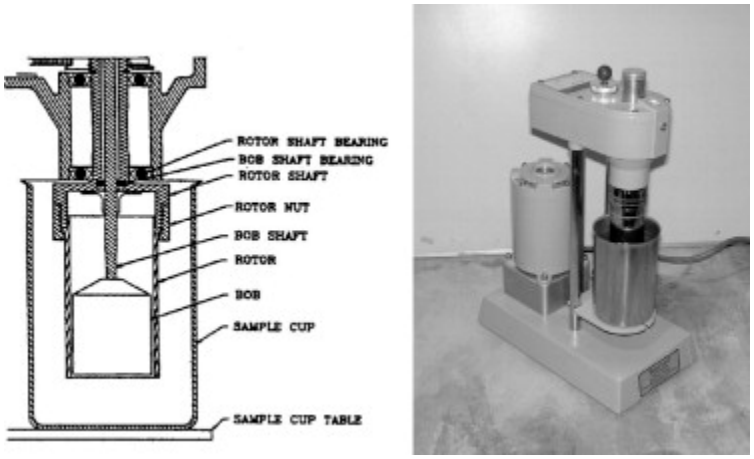

Figure 3-2: The coaxial cylinder viscometer is a rotational viscometer that contains a stationary inner cylinder, "bob", and a rotating outer cylinder, "cup". The image on the left labels the different components while the image on the right shows a real image of the viscometer. Taken from [35].

The cone and plate viscometer is also a rotational viscometer and is similar to the coaxial cylinder viscometer. Instead of a "bob" and "cup", it is comprised of a cone and flat plate. When the cone is placed on top of the flat plate, a small angle is made relative to the plate. This angle is assumed to be small enough to make the small angle approximation. The shear rate is the ratio of the linear velocity, Ωr, and the gap between the cone and plate, rtanα or rα by small angle approximation. The shear rate simplifies to Ω/α [33].

The total torque is governed by:

T = $\int_0^R 2\pi r^2 \tau_r dr$, where τ_r is the shear stress.

For a Newtonian fluid,

$$\mu = \frac{3T\alpha}{2\pi R^3 \Omega}$$

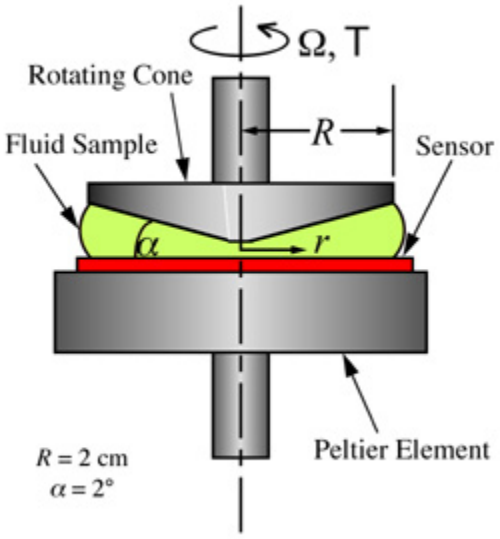

Figure 3-3: The cone and plate viscometer is another type of rotational viscometer that utilizes a cone and a flat plate. Taken from [36]

Each viscometer has a set of advantages and disadvantages. The capillary viscometer gives results that are reproducible and requires a small volume of fluid. However, it does not expose the tube to a constant shear stress and thus may not be applicable for non-Newtonian fluids. The coaxial cylinder viscometer subjects the fluid sample to a constant shear rate and measurements can be taken at various shear rates. The cone and plate viscometers are similar to the coaxial cylinder viscometers in their relative advantages. However, the cone and plate viscometer is more widely used due to accuracy. Based on the comparison of the viscometers, the cone and plate viscometer seems to be the optimal viscometer to use to conduct the experiment to validate the results [33].

Chapter 4: Conclusion

In Figure 1-16, experimental data of the selectivity and the Stokes-Einstein-Sutherland Equation were plotted against the molecular weight ratio. Based on the figure, it can be seen that there both plots follow a similar trend. The SES equation, however, over predicts the selectivity at low molecular weight ratios and under predicts it at high molecular weight ratios. The goal of the project is to correct the discrepancy shown in the figure.

Equation (2) assumes that the viscosity ratio of the i^{th} protein and the j^{th} protein is equal. So the equation simply reduces to the negative cube root of the molecular weight ratio. This was the equation that was used to generate the dashed curve in Figure 1-16. The initial assumption made in this project was that the viscosity ratio is not constant. This can be explained by the crowding effect phenomenon at the interphase, where the proteins compete to adsorb onto the surface.

Various models such as the Einstein's Viscosity Model, Hatschek's Viscosity Model, and Cokelet's Viscosity Model were substituted in for the viscosity ratio in the SES Equation. But they all failed to fit the data. Then the viscosity ratio was modeled using standard equations such as linear and exponential functions. The exponential function depicted by Equation (20) fit the data both qualitatively and quantitatively.

The equation implies that the viscosity of protein *i* increases relative to that of protein *j* with increasing molecular weight ratios. This can be validated by using a cone and plate viscometer to measure the viscosity of the i^{th} and j^{th} proteins at different concentrations and a subsequent substitution of the viscosity values into Equation (6).

Appendices

Appendix A: Derivation of the hydration sphere

Molecular volume of a hypothetical protein sphere:

$V_p = \frac{4}{3}\pi r_v^3$, where r_v is the molecular radius (cm/molecule).

Molar Volume:

$$\bar{V_p} = \frac{4}{3}\pi r_v^3 N_A$$

Where N_A is the Avogadro number.

The specific volume is:

$$v^o = \bar{V_p} * MW * 10^3 \ (\frac{cm^3}{g})$$

Where MW is the molecular weight in kDa

Using the relationship, $r_v = 6.72 \times 10^{-8}\ MW^{1/3}$ and substituting $\bar{V_p}$ into v^o gives:

$$v^o = \frac{4}{3}\pi N_A \frac{\left(6.72\ x\ 10^{-8} * MW^{\frac{1}{3}}\right)^3}{10^3 * MW}$$

$$v^o = \frac{4}{3}\pi(6.02\ x\ 10^{23})\frac{\left(6.72\ x\ 10^{-8}\right)^3}{10^3} = 0.77\frac{cm^3}{g}$$

$$v^o = 0.77\frac{cm^3}{g}$$

Appendix B: Proteins used in Single Solution experiment

Protein (Origin)	Molecular Weight (kDa)	Purity (electrophoresis) or activity	Vendor	As-received form
Lysozyme (human neutrophils)	15	> 95%	Sigma-Aldrich	Powder
α-Amylase (human saliva)	51	1920 units/mg	Sigma-Aldrich	Powder
Human serum albumin (human blood)	66.3	96 - 99%	Sigma-Aldrich	Powder
Prothrombin (human blood)	72	90 µg/unit	Enzyme research	Powder
Human IgG (human blood)	160	> 95%	Sigma-Aldrich	Powder
Fibrinogen (human blood)	341	80% clottable protein	Sigma-Aldrich	Powder

Appendix C: Proteins used in Binary Solution experiment

Name of protein (acronym)	Molecular weight (kDa)	As-received form	Purity (electrophoresis) or activity	Vendor
Ubiquitin (Ub)	10.7	Powder	98%	Sigma Aldrich
Human serum albumin (HSA)	66.3	Powder	96–99%	Sigma Aldrich
Prothrombin (FII)	72	Powder	>95%	Enzyme research
Human IgG (IgG)	160	Powder	>95%	Sigma Aldrich
Fibrinogen (Fib)	341	Powder	80% Clottable protein	Sigma Aldrich

Appendix D: Selectivity results from Binary Solution experiment

rotein Pairs	on dit io n				State 1			State 2			ransiti on Period (min)	$i,j(N,R^2$)
					$D_i)_{i,j}$ mg /mL, (N)	$D_j)_{i,j}$ mg /mL, (N)	$Dj)_{i,j}/(Di)_{i,j}$	$D_i)_{i,j}$ mg /mL, (N)	$D_j)_{i,j}$ mg /mL, (N)	$Dj)_{i,j}/(Di)_{i,j}$		
SA (i) + Fib (j)	as e 1	.25	.25	.0 0	.66 ± 0. 05, (9)	.46 ± 0. 05, (9)	.70 ± 0 .09	.53 ± 0. 05, (3)	.28 ± 0. 03, (3)	.53 ± 0 .08	5–75	.80 ± 0 .02 (5, 0.99)
	as e 2	.00	.00	.5 0	.98 ± 0. 06, (9)	.21 ± 0. 08, (9)	.23 ± 0 .11	.60 ± 0. 01, (3)	.74 ± 0. 01, (3)	.23 ± 0 .03	5–80	
	as e 3	.00	.00	.5 0	.61 ± 0. 09, (9)	.60 ± 0. 03, (9)	.37 ± 0 .02	.11 ± 0. 09, (6)	.45 ± 0. 04, (5)	.41 ± 0 .05	5–70	
	as e 4	.00	.50	.2 5	.96 ± 0. 05, (9)	.60 ± 0. 11, (7)	.71 ± 0 .18	.62 ± 0. 05, (4)	.01 ± 0. 03, (4)	.24 ± 0 .26	0–75	
	as e 5	.00	.50	.6 2	.34 ± 0. 07, (6)	.86 ± 0. 13, (5)	.22 ± 0 .26	.57 ± 0. 05, (5)	.14 ± 0. 04, (3)	.36 ± 0 .05	5–80	
SA (i) + IgG (j)	ase 1	.25	.25	.0 0	.56 ± 0. 03, (9)	.52 ± 0. 03, (8)	.94 ± 0 .07	.36 ± 0. 02, (4)	.35 ± 0. 02, (3)	.97 ± 0 .08	0–80	.88 ± 0 .03 (5, 0.99)
	ase 2	.08	.00	.4 0	.12 ± 0. 06, (8)	.20 ± 0. 14, (8)	.96 ± 0 .16	.90 ± 0. 05, (4)	.58 ± 0. 11, (4)	.76 ± 0 .16	0–75	
	ase 3	.17	.00	.2 0	.21 ± 0. 09, (6)	.02 ± 0. 16, (6)	.91 ± 0 .08	.64 ± 0. 10, (3)	.75 ± 0. 04, (3)	.17 ± 0 .19	5–80	
	ase 4	.08	0.0 0	.8 1	.92 ± 0. 04, (7)	.04 ± 0. 17, (7)	.39 ± 0 .26	.69 ± 0. 01, (4)	.75 ± 0. 08, (4)	.98 ± 0 .13	5–80	

rotein Pairs	on dit io n				State 1			State 2			ransiti on Period (min)	*i*,*j*(*N*,R^2)
					$D_{i})_{i,j}$ mg /mL, (N)	$D_{j})_{i,j}$ mg /mL, (N)	$Dj)_{i,j}/(Di)_{i,j}$	$D_{i})_{i,j}$ mg /mL, (N)	$D_{j})_{i,j}$ mg /mL, (N)	$Dj)_{i,j}/(Di)_{i,j}$		
	ase 5	.17	0.0 0	.4 0	.26 ± 0. 22, (9)	.35 ± 0. 15, (5)	.92 ± 0 .20	.92 ± 0. 14, (3)	.10 ± 0. 23, (4)	.28 ± 0 .43	0–85	
SA (i) + Ub (j)	ase 1	.33	.25	.9 4	.67 ± 0. 02, (7)	.66 ± 0. 01, (9)	.98 ± 0 .03	.55 ± 0. 00, (3)	.48 ± 0. 01, (5)	.87 ± 0 .02	0–75	.09 ± 0 .04 (3, 0.98)
	ase 3	.00	.08	.4 2	.29 ± 0. 09, (9)	.00 ± 0. 06, (8)	.44 ± 0 .03	.30 ± 0. 03, (4)	.60 ± 0. 03, (5)	.46 ± 0 .02	0–75	
	ase 5	.00	.00	.0 0	.18 ± 0. 29, (8)	.49 ± 0. 12, (5)	.14 ± 0 .16	.96 ± 0. 09, (4)	.86 ± 0. 10, (6)	.90 ± 0 .13	5–65	
gG (i) + Fib (j)	ase 1	.00	.50	.5 0	.22 ± 0. 06, (13)	.55 ± 0. 03, (13)	.45 ± 0 .03	.94 ± 0. 04, (4)	.41 ± 0. 02, (4)	.43 ± 0 .03	5–80	.90 ± 0 .01 (3, 1.00)
	ase 3	0.0 0	.50	.2 5	.02 ± 0. 37, (10)	.97 ± 0. 06, (10)	.24 ± 0 .03	.60 ± 0. 14, (3)	.71 ± 0. 01, (3)	.27 ± 0 .02	5–80	
	ase 5	0.0 0	.00	.7 0	.89 ± 0. 22, (9)	.06 ± 0. 14, (9)	.63 ± 0 .04	.33 ± 0. 22, (3)	.27 ± 0. 10, (3)	.68 ± 0 .05	5–80	
II (i) + Fib (j)	ase 1	.50	.25	.8 3	.74 ± 0. 04, (11)	.55 ± 0. 03, (11)	.74 ± 0 .06	.31 ± 0. 03, (4)	.25 ± 0. 04, (4)	.81 ± 0 .15	5–75	.96 ± 0 .06 (3, 0.96)
	ase 3	.00	.50	.4 2	.05 ± 0. 18, (17)	.04 ± 0. 10, (17)	.34 ± 0 .11	o State 2	o State 2			
	ase 5	.00	.00	.1 7	.35 ± 0. 10, (10)	.79 ± 0. 11, (10)	.19 ± 0 .07	.40 ± 0. 19, (4)	.86 ± 0. 03, (4)	.33 ± 0 .18	0–75	
II (i) +	ase 1	.50	.50	.0 0	.64 ± 0. 04, (18)	.70 ± 0. 04, (18)	.09 ± 0 .09	No State 2			o State	.97 ± 0 .06 (3,

rotein Pairs	on dit io n				State 1			State 2			ransiti on Period (min)	*i*,*j*(*N*,R^2)
					$D_{i})_{i,j}$ mg /mL, (N)	$D_{j})_{i,j}$ mg /mL, (N)	$Dj)_{i,j}$/($Di)_{i,j}$	$D_{i})_{i,j}$ mg /mL, (N)	$D_{j})_{i,j}$ mg /mL, (N)	$Dj)_{i,j}$/($Di)_{i,j}$		
IgG (j)											2	0.96)
	ase 3	.00	.00	.5 0	.60 ± 0. 11, (15)	.17 ± 0. 09, (17)	.45 ± 0 .04	No State 2			o State 2	
	ase 5	.00	0.0 0	.6 7	.46 ± 0. 15, (8)	.81 ± 0. 20, (8)	.55 ± 0 .12	.10 ± 0. 08, (6)	.01 ± 0. 15, (6)	.83 ± 0 .19	0–65	

Reversed protein pairs (from Table 2A)	Experimental condition	$\overline{S}_{i,j}(N, R^2$	$S_{i,j}$ (N, R^2)
HSA (j) + Fib (i)	Case 1	1.35 ± 0.03 (5, 0.99)	0.80 ± 0.02 (5, 0.99)
	Case 2		
	Case 3		
	Case 4		
	Case 5		
HSA (j) + IgG (i)	Case 1	1.18 ± 0.06 (5, 0.95)	0.88 ± 0.03 (5, 0.99)
	Case 2		
	Case 3		
	Case 4		
	Case 5		
HSA (j) + Ub (i)	Case 1	0.94 ± 0.02 (3, 1.00)	1.09 ± 0.04 (3, 0.98)
	Case 3		
	Case 5		
IgG (j) + Fib (i)	Case 1	1.06 ± 0.02 (3, 0.99)	0.90 ± 0.01 (3, 1.00)
	Case 3		
	Case 5		
FII (j) + Fib (i)	Case 1	1.19 ± 0.06 (3, 0.98)	0.96 ± 0.06 (3, 0.96)
	Case 3		
	Case 5		
FII (j) + IgG (i)	Case 1	1.07 ± 0.05 (3, 0.98)	0.97 ± 0.06 (3, 0.96)

Appendix E: Derivation of the Stokes – Einstein – Sutherland Equation

For low Reynolds number, the drag force is proportional to a particle's velocity.

$F_D = K * v$, where K is a translation tensor and v is the velocity.

The components of K are referred to as the friction coefficients f_{ij}. K is a symmetric tensor that can be expressed in terms of the principal friction coefficients: f_1, f_2, and f_3. So it can be said that:

$$F_D = \frac{f}{v}$$

$$v = \frac{F_D}{f}$$

In one dimension, the force balance is:

$$m_p \frac{d^2x}{dt^2} = -\frac{f dx}{dt} + F_T$$

Assuming that F_T is a random variable with a zero mean and then multiplying by x, the left side can be rewritten as:

$$x\frac{d^2x}{dt^2} = \frac{d}{dt}\left(x\frac{dx}{dt}\right) - \left(\frac{dx}{dt}\right)^2$$

$$\frac{1}{2}m_p\frac{d}{dt}\left(\frac{dx^2}{dt}\right) - m_p\frac{d^2x}{dt^2} = -\frac{f dx^2}{2dt}$$

The kinetic energy of a particle moving in one dimension is equal to the thermal energy, k_BT, where k_B is the Boltzmann's Constant and T is the temperature. Setting $\frac{dx^2}{dt}$ to 0 results in:

$$x^2 = \frac{2k_BT}{f}t - 2\frac{m_p k_B T}{\bar{f}^2}\left(1 - \exp\left(-\frac{\bar{f}t}{m_p}\right)\right.$$

This then becomes:

$D_{ij} = \frac{k_B T}{f}$, where *f* is the friction factor. For a sphere, f is $6\pi\eta R$.

$$D_{ij} = \frac{k_B T}{6\pi\eta R}$$

REFERENCES

[1] Vogler, Erwin A. "Surfaces and the Biological (Host) Response to Materials." BioE 517. The Pennsylvania State University. Aug. 2010. Lecture.

[2] Vogler, Erwin A. "Biomaterials: A Field at the Intersection of Disciplines." BioE 517. The Pennsylvania State University. Sept. 2010. Lecture.

[3]Vogler EA. Interfacial chemistry in biomaterials science. In: Berg J, editor. Wettability. New York: Marcel Dekker; 1993. p. 184e250.

[4] Aveyard R, Haydon DA. An introduction to the principles of surface chemistry. London: Cambridge University Press; 1973.

[5] Vogler EA. Structure and reactivity of water at biomaterial surfaces. Adv Colloid Interface 1998;74:69e117.

[6] Rosen MJ. Surfactants and interfacial phenomena. New York: Wiley; 1978.

[7] "Absorption vs Adsorption." - *Difference and Comparison*. N.p., n.d. Web. 1 Dec. 2012.

[8] Gibbs JW. The scientific papers of J. Willard Gibbs. New York: Dover Publications; 1961.

[9] Guggenheim EA. In: Thermodynamics: an advanced treatment for chemists and physicists. 5th ed. New York: Wiley; 1967.

[10] Hofmeister F. zur lehre von der wirkung der salze (to the theory of the effect of salts). Archiv fur Experimentelle Pathologie und Pharmakologie (Arch Exp Path Pharm) 1888;24:247e69.

[11] Anderson NL, Anderson NG. The human plasma proteome: history, character, and diagnostic prospects. Mol Cell Proteomics 2002;1:845e67.

[12] Richards FM. Areas, volumes, packing and protein structure. Ann Rev Biophys Bioeng 1977;6:151e76.

[13] Chothia C. Structural invariants in protein folding. Nature 1975;254:304e8.

[14] Miller S, Lesk A, Janins J, Chothia C. The accessible surface area and stability of oligomeric proteins. Nature 1987;328:834e6.

[15] Miller S, Janin J, Lesk A, Chothia C. Interior and surface of monomeric proteins. J Mol Biol 1987;196:641e56.

[16] Tsai J, Taylor R, Chothia C, Gerstin M. The packing density in proteins: standard radii and volumes. J Mol Bio 1999;290:253e66.

[17] Vogler EA. Proteins in three dimensions. Biomaterials.p.1201-1237. 2012.

[18] Horbett T. Protein Adsorption on Biomaterials. In: Cooper SL, Peppas NA, Hoffman AS, Ratner BD, editors. Biomaterials: Interfacial Phenomena and Applications. Washington D. C.: Am. Chem. Soc.; 1982. pp. 234–243.

[19] Tripp BC, Magda JJ, Andrade JD. Adsorption of Globular Proteins at the Air/Water Interface as Measured via Dynamic Surface Tension: Concentration Dependence, Mass-transfer Considerations, and Adsorption Kinetics. J Colloid and Interface Sci. 1995;173:16–27.

[20] Ward AFH, Tordai L. Time-Dependence of Boundary Tensions of Solutions I. The Role of Diffusion in Time-Effects. J Chem Phys. 1946;14(7):453–461

[21] Barnthip N. Volumetric Interpretation of Protein Adsorption: Kinetic Consequences of a Slowly-Concentrating Interphase. Biomaterials. P.3062-3074. 2008.

[22] Noh H, Vogler EA. Volumetric interpretation of protein adsorption: mass and energy balance for albumin adsorption to particulate adsorbents with incrementally increasing hydrophilicity. Biomaterials. P.5801-5812. 2008.

[23] Barnthip N, Parhi P, Golas A, Vogler EA. Volumetric interpretation of protein adsorption: kinetics of protein-adsorption competition from binary solution. Biomaterials 2009;30:6495e513.

[24] Truskey, George A., Fan Yuan, and David F. Katz. "The Stokes Einstein Equation." *Transport Phenomena in Biological Systems*. Upper Saddle River, NJ: Pearson Prentice Hall, 2009. N. pag. Print.

[25] "What's a Good Value for R-squared?" *What's a Good Value for R-squared?* Duke, n.d. Web. 12 Jan. 2013.

[26] Zydney AL. A constitutive equation for the viscosity of stored red cell suspensions: Effect of hematocrit, shear rate, and suspending phase. Journal of Rheology. 1991. p.1639e1680.

[27] Thurston, G. B., "Effects of Hematocrit on Blood Viscoelasticity and in Establishing Normal Values," Biorheol. 15, 239-49 (l978).

[28] Thurston, G. 8., "Erythrocyte Rigidity as a Factor in Blood Rheology: Viscoelastic Dilatancy," J. Rheol. 23, 703-19 (1979).

[29] Merrill, E. W., A. M. Benis, E. R. Gilliland, T. K. Sherwood, and E. W. Salzman, "Pressure-Flow Relations of Human Blood in Hollow Fibers at Low Flow Rates," J. Appl. Physiol. 20, 954--67 (1965).

[30] Hughes AJ. The Einstein Relation between Relative Viscosity and Volume Concentration of Suspensions of Spheres. Nature. 1089-1090. 1954.

[31] Hatschek E. The general theory of viscosity of two-phase systems. p.80-92. 1913.

[32] Farrow FD., Lowe GM., The Flow of Starch Paste Through Capillary Tubes. J. Textile Institute Transactions, 14:11,T414-T440. 1923.

[33] Chandran, K. B., Stanley E. Rittgers, and A. P. Yoganathan. *Biofluid Mechanics: The Human Circulation*. Boca Raton: CRC/Taylor & Francis, 2007. Print.

[34] "Capillary Viscometer." *Http://ciks.cbt.nist.gov*. NIST, n.d. Web.

[35] "Coaxial Cylinder Viscometer." *Http://ars.els-cdn.com/content*. N.p., n.d. Web.

[36] "Main Page." *SoftMatter RSS*. N.p., n.d. Web. 26 Mar. 2013.

ACADEMIC VITA

Sai K. Sunkara

215 B South Valley Forge road, Devon, PA 19333/sks5201@psu.edu

---

Education

B.S., Bioengineering, 2013, The Pennsylvania State University, University Park, PA

B.S., Mechanical Engineering, 2013, The Pennsylvania State University, University Park, PA

Honors and Awards

I was on the Dean's List because I maintained a GPA of over 3.50 every semester that I was at Penn State. I was also awarded the summer undergraduate research fellowship at the National Institute of Standards and Technology in 2011.

Association Memberships/Activities

- Biomedical Engineering Society
- Tau Beta Pi
- Society of Hispanic Professional Engineers

Research Interests

My future research interests include device development. I constantly brainstorm potential ideas that I can implement. Recently, an idea that is of particular interest is the development of universal glucose strips. I am recruiting engineers within the Bioengineering, Electrical, and Material Science and Engineering Departments to carry out the project. At the University of Pennsylvania, I would like to further develop my interest in device design and development.

Professional Presentations

Title: Characterization of the NIST Reference Scaffolds to enable inter lab comparison of cell culture measurements

Location: National Institute of Standards and Technology (NIST)

Audience: NIST Scientists

Date: 08/09/2011

Publications and Papers

The successful correction of the Stokes-Einstein-Sutherland Equation will lead to a publication according to Dr. Vogler. There is also a chance that a paper will be written for the development of a low cost Ears, Nose, and Throat Scope by my group in the junior Bioengineering Design Class, BioE 401.